Chapter 4

Quaternion, Harmonic Oscillator, and High-Dimensional Topological States

Congjun Wu
Department of Physics, University of California, San Diego, CA 92093, USA
wucj@physics.ucsd.edu

Quaternion, an extension of complex number, is the first discovered non-commutative division algebra by William Rowan Hamilton in 1843. In this chapter, we review the recent progress in building up the connection between the mathematical concept of quaternionic analyticity and the physics of high-dimensional topological states. Three- and four-dimensional harmonic oscillator wavefunctions are organized by the SU(2) Aharonov–Casher gauge potential to yield high-dimensional Landau levels possessing the full rotational symmetries and flat energy dispersions. The lowest Landau-level wavefunctions exhibit quaternionic analyticity, satisfying the *Cauchy–Riemann–Fueter* condition, which generalizes the two-dimensional complex analyticity to three and four dimensions. It is also the Euclidean version of the helical Dirac and the chiral Weyl equations. After dimensional reductions, these states become two- and three-dimensional topological states maintaining time-reversal symmetry but exhibiting broken parity. We speculate that quaternionic analyticity can provide a guiding principle for future researches on high-dimensional interacting topological states. Other progresses including high-dimensional Landau levels of Dirac fermions, their connections to high-energy physics, and high-dimensional Landau levels in the Landau-type gauges, are also reviewed. This research is also an important application of the mathematical subject of quaternion analysis to theoretical physics, and provides useful guidance for the experimental explorations on novel topological states of matter.

4.1 Introduction

I feel honored to contribute to this memorial volume for Professor Shoucheng Zhang. As one of his former Ph.D. students, I have been deeply influenced by his insights and tastes on physics along my research career. Shoucheng expressed that he liked our work on quaternion analyticity and high-dimensional Landau levels. Hence, I review the progress in this direction below.

Quaternions, also called Hamilton numbers, are the first noncommutative division algebra as a natural extension to complex numbers (see the quaternion plaque in Fig. 4.1). Imaginary quaternion units i, j and k are isomorphic to the anti-commutative SU(2) Pauli matrices $-i\sigma_{1,2,3}$. Hamilton used quaternions to represent three-dimensional (3D) and four-dimensional (4D) rotations, and performed the product of two rotations based on the quaternion multiplication. In fact, it is amazing that he was well ahead of his time — equivalently he was using the spin-$\frac{1}{2}$ fundamental representations of the SU(2) group, which was before quantum mechanics was discovered. Nevertheless, the development of quaternoinic analysis met significant difficulty since quaternions do not commute. An important progress was made by Fueter in 1935 as reviewed in [1] who defined the Cauchy–Riemann–Fueter condition for quaternionic analyticity. Amazingly again, this is essentially the Euclidean version of the Weyl equation proposed in 1929. Later on, there have been considerable efforts in constructing quantum mechanics and quantum field theory based on quaternions [2–4].

On the other hand, the past decade has witnessed a tremendous progress in the study of topological states of matter, in particular, time-reversal invariant topological insulators in two dimensions (2D) and 3D. Topological properties of their band structures are characterized by a $\mathbb{Z}_2$-index, which are stable against time-reversal invariant perturbations and weak interactions [5–15]. These studies are further developments of quantum anomalous Hall insulators characterized by the integer-valued Chern numbers [16, 17]. Later on, topological states of matter including both insulating and superconducting states have been classified into ten different classes in terms of their properties under the chiral, time-reversal, and particle–hole symmetries [18, 19]. These studies have mostly focused on lattice systems. The wavefunctions of the Bloch bands are complicated, and their energy spectra are dispersive, both of which are obstacles for the study of high-dimensional fractional topological states.

In contrast, the 2D quantum Hall states [20, 21] are early examples of topological states of matter studied in condensed matter physics. They arise from the Landau-level quantization due to the cyclotron motion of electrons in a magnetic field [22]. Their wavefunctions are simple and elegant, which are basically harmonic oscillator wavefunctions. They are reorganized to exhibit analytic properties by an external magnetic field.

Generally speaking, a 2D quantum mechanical wavefunction $\psi(x, y)$ is complex valued, but not necessarily complex analytic. We do not need the whole set of 2D harmonic oscillator wavefunctions, but would like to select a subset of them with nontrivial topological properties, then complex analyticity is a natural selection criterion. Indeed, the lowest Landau-level wavefunctions exhibit complex analyticity. Mathematically, it is imposed by the Cauchy–Riemann condition (see Eq. (4.4) in the text), and physically it is implemented by a magnetic field, which reflects the fact that the cyclotron motion is chiral. This fact greatly facilitated the construction of the Laughlin wavefunction in the study of fractional quantum Hall states [23].

How to generalize Landau levels to 3D and even higher dimensions is a challenging question. A pioneering work was done by Shoucheng and his former student Jiangping Hu in 2001 [24]. They constructed the Landau-level problem on the compact space of an S^4 sphere, which generalizes Haldane's formulation of the 2D Landau levels on an S^2 sphere. Haldane's construction is based on the first Hopf map [25], in which a particle is coupled to the vector potential from a $U(1)$ magnetic monopole. Zhang and Hu considered a particle lying on the S^4 sphere coupled to an SU(2) monopole gauge field, and employed the second Hopf map which maps a unit vector on an S^4 sphere to a normalized 4-component spinor. The Landau-level wavefunctions are expressed in terms of the four components of the spinor. Such a system is topologically nontrivial characterized by the second Chern number possessing time-reversal symmetry. This construction is very beautiful, however, it needs significantly advanced mathematical physics knowledge which may not be common for the general readers in the condensed matter physics, and atomic, molecular, and optical physics community.

We have constructed high-dimensional topological states (e.g., 3D and 4D) based on harmonic oscillator wavefunctions in flat spaces [26, 27]. They exhibit flat energy dispersions and nontrivial topological properties, hence, they are generalizations of the 2D Landau-level problem to high dimensions. Again we will select and reorganize a subset of wavefunctions in seeking for nontrivial topological properties. The strategy we employ is to use quaternion analyticity as the new selection criterion to replace the previous one of complex analyticity. Physically, it is imposed by spin–orbit coupling, which couples orbital angular momentum and spin together to form the helicity structure. In other words, the helicity generated by spin–orbit coupling plays the role of 2D chirality due to the magnetic field. Our proposed Hamiltonians can also be formulated in terms of spin-$\frac{1}{2}$ fermions coupled to an SU(2) gauge potential, or, an Aharonov–Casher potential. Gapless helical Dirac surface modes, or, chiral Weyl modes, appear on open boundaries manifesting the nontrivial topology of bulk states.

We have also constructed high-dimensional Landau levels of Dirac fermions [28], whose Hamiltonians can be interpreted in terms of complex quaternions. The zeroth Landau levels of Dirac fermions are a branch of half-fermion Jackiw–Rebbi modes [29], which are degenerate over all the 3D angular momentum quantum numbers. Unlike the usual parity anomaly and chiral anomaly in which massless Dirac fermions are minimally coupled to the background gauge fields, these Dirac Landau-level problems correspond to a nonminimal coupling between massless Dirac fermions and background fields. This problem lies at the interfaces among condensed matter physics, mathematical physics, and high-energy physics.

High-dimensional Landau levels can also be constructed in the Landau-type gauge, in which rotational symmetry is explicitly broken [30]. The helical, or, chiral plane-waves are reorganized by spatially dependent spin–orbit coupling to yield nontrivial topological properties. The 4D quantum Hall effect of the SU(2) Landau levels has also been studied in the Landau-type gauge, which exhibits the quantized nonlinear electromagnetic response as a spatially separated 3D chiral anomaly.

We speculate that quaternionic analyticity would act as a guiding principle for studying high-dimensional interacting topological states, which is a major challenging question. The high-dimensional Landau-level problems reviewed below provide an ideal platform for this research. This research is at the interface between mathematical and condensed matter physics, and has potential benefits to both fields.

This chapter is organized as follows. In Sec. 4.2, histories of complex number and quaternion, and the basic knowledge of complex analysis and quaternion analysis are reviewed. In Sec. 4.3, the 2D Landau-level problems are reviewed for both nonrelativistic particles and relativistic particles. The complex analyticity of the lowest Landau-level wavefunctions is presented. In Sec. 4.4, the constructions of high-dimensional Landau levels in 3D and 4D with explicit rotational symmetries are reviewed. The quaternionic analyticity of the lowest Landau-level wavefunctions, and the bulk–boundary correspondences in terms of the Euclidean and Minkowski versions of the Weyl equation are presented. In Sec. 4.5, we review the dimensional reductions from the 3D and 4D Landau-level problems to yield the 2D and 3D isotropic but parity-broken Landau levels, respectively. They can be constructed by combining a harmonic potential and a linear spin–orbit coupling. In Sec. 4.6, the high-dimensional Landau levels of Dirac fermions are constructed, which can be viewed as Dirac equations in phase spaces. They are related to gapless Dirac fermions nonminimally coupled to background fields. In Sec. 4.7, high-dimensional Landau levels in the anisotropic Landau-type gauge are reviewed. The 4D quantum Hall responses are derived as a spatially separated chiral anomaly. Conclusions and outlooks are presented in Sec. 4.8.

4.2 Histories of complex number and quaternion

4.2.1 *Complex number*

Complex number plays an essential role in mathematics and quantum physics. The invention of complex number was actually related to the history of solving the algebraic cubic equations, rather than solving the quadratic equation of $x^2 = -1$. If one lived in the 16th century, one could simply say that such an equation has no solution. But cubic equations are different. Consider a reduced cubic equation $x^3 + px + q = 0$, which can be solved by using radicals. Here is the Cardano formula,

$$x_1 = c_1 + c_2, \quad x_2 = c_1 e^{i\frac{2\pi}{3}} + c_2 e^{-i\frac{2\pi}{3}}, \quad x_3 = c_1 e^{-i\frac{2\pi}{3}} + c_2 e^{i\frac{2\pi}{3}}, \tag{4.1}$$

where

$$c_1 = \sqrt[3]{-\frac{q}{2} + \sqrt{\Delta}}, \quad c_2 = \sqrt[3]{-\frac{q}{2} - \sqrt{\Delta}}, \tag{4.2}$$

with the discriminant $\Delta = (\frac{q}{2})^2 + (\frac{p}{3})^3$. The key point of the expressions in Eq. (4.1) is that they involve complex numbers. For example, consider a cubic equation with real coefficients and three real roots $x_{1,2,3}$. It is purely a real problem: It starts with real coefficients and ends up with real solutions. Nevertheless, it can be proved by the Galois theory that there is no way to bypass i. Complex conjugate numbers appear in the intermediate steps, and finally they cancel to yield real solutions. As a concrete example, for the case that $p = -9$ and $q = 8$, complex numbers are unavoidable since $\sqrt{\Delta} = \sqrt{-11}$. The readers may check how to arrive at three real roots of $x_{1,2,3} = 1, -\frac{1}{2} \pm \frac{\sqrt{33}}{2}$.

Once the concept of complex number was accepted, it opened up an entire new field for both mathematics and physics. Early developments include the geometric interpretation of complex numbers in terms of the Gauss plane, the application of complex numbers for two-dimensional rotations, and the Euler formula

$$e^{i\theta} = \cos\theta + i\sin\theta. \tag{4.3}$$

The complex phase appears in the Euler formula, which is widely used in describing mechanical and electromagnetic waves in classic physics, and also quantum mechanical wavefunctions. Moreover, when a complex-valued function $f(x, y)$ satisfies the Cauchy–Riemann condition,

$$\frac{\partial f}{\partial x} + i\frac{\partial f}{\partial y} = 0, \tag{4.4}$$

it only depends on $z = x + iy$ but not on $\bar{z} = x - iy$. The Cauchy–Riemann condition sets up the foundation of complex analysis, giving rise to the Cauchy integral,

$$\frac{1}{2\pi i}\oint \frac{1}{z - z_0} dz f(z) = f(z_0). \tag{4.5}$$

For physicists, a practical use of complex analysis is to calculate loop integrals. Certainly, its importance is well beyond this. Complex analysis is the basic tool for many modern branches of mathematics. For example, it gives rise to the most elegant proof to *the fundamental theorem of algebra*: An algebraic equation $f(z) = 0$, i.e., $f(z)$ is an nth-order polynomial of z, has n complex roots. The proof is essentially to count the phase winding number of $1/f(z)$ as moving around a circle of radius $R \to +\infty$. On this circle, $1/f(z) \to z^{-n}$, then the winding number simply equals $-n$. On the other hand, the winding number is a topological invariant equal to the negative of the number of poles of $1/f(z)$. Hence, n equals the number of zeros of $f(z)$. Complex analysis is also the basic tool of number theory: The Riemann hypothesis, which aims at studying the distribution of prime numbers, is formulated as a complex analysis problem of the distributions of the zeros of the Riemann $\zeta(z)$-function.

Complex numbers actually are inessential in the entire scope of classical physics. It is well known that the complex number description for classic waves is only a convenience but not necessary. The first time that complex numbers are necessary is in quantum mechanics — the Schrödinger equation,

$$i\hbar\partial_t \psi = H\psi. \tag{4.6}$$

In contrast, classic wave equations only involve ∂_t^2, and i disappears since its square equals -1. In fact, Schrödinger attempted to eliminate i in his equation, but did not succeed. Hence, to a certain extent, i, or, the complex phase, is more important than $\hbar$ in quantum physics.

4.2.2 *Quaternion and quaternionic analyticity*

Since 2D rotations can be elegantly described by the multiplication of complex numbers, it is reasonable to expect that 3D rotations could also be described in a similar way by extending complex numbers to include the third dimension. Simply adding another imaginary unit j to construct $x + yi + zj$ does not work, since the product of two imaginary units $ij \neq i \neq j \neq \pm 1$.

Fig. 4.1. The quaternion plaque on Brougham Bridge, Dublin. From wikipedia, https://en.wikipedia.org/wiki/History_of_quaternions.

It has to be a new imaginary unit defined as $k = ij$, and then the quaternion is constructed as

$$q = x + yi + zj + uk. \tag{4.7}$$

The quaternion algebra,

$$i^2 = j^2 = k^2 = ijk = -1, \tag{4.8}$$

was invented by Hamilton in 1843 when he passed the Brougham bridge in Dublin (see Fig. 4.1). He realized in a genius way that the product table of the imaginary units cannot be commutative. In fact, it can be derived based on Eq. (4.8) that i, j, and k anti-commute with one another, i.e.,

$$ij = -ji, \quad jk = -kj, \quad ki = -ik. \tag{4.9}$$

This is the first noncommutative division algebra discovered, and actually it was constructed before the invention of the concept of matrix. In modern mathematical language, quaternion imaginary units are isomorphic to the Pauli matrices $-i\sigma_1, -i\sigma_2, -i\sigma_3$.

Hamilton employed quaternions to describe the 3D rotations. Essentially he used the spin-$\frac{1}{2}$ spinor representation: Consider a 3D rotation R around the axis along the direction of $\hat{\Omega}$ and the rotation angle is γ. Define a unit imaginary quaternion,

$$\omega(\hat{\Omega}) = i \sin\theta \cos\phi + j \sin\theta \sin\phi + k \cos\theta, \tag{4.10}$$

where θ and ϕ are the polar and azimuthal angles of $\hat{\Omega}$. Then the unit quaternion associated with such a rotation is defined as

$$q = \cos\frac{\gamma}{2} + \omega(\hat{\Omega})\sin\frac{\gamma}{2}, \tag{4.11}$$

which is essentially an SU(2) matrix. A 3D vector $\vec{r}$ is mapped to an imaginary quaternion $r = xi + yj + zk$. After the rotation, $\vec{r}$ is transformed to $\vec{r}'$, and its quaternion form is

$$r' = qrq^{-1}. \tag{4.12}$$

This expression defines the homomorphism from SU(2) to SO(3). In fact, using quaternions to describe rotation is more efficient than using the 3D orthogonal matrix, hence, quaternions are widely used in computer graphics and aerospace engineering even today. If set $\vec{r} = \hat{z}$ in Eq. (4.12), and let q run over unit quaternions, which span the S^3 sphere, then a mapping from S^3 to S^2 is defined as

$$n = qkq^{-1}, \tag{4.13}$$

which is the first Hopf map.

Hamilton spent the last 20 years of his life to promote quaternion applications [8]. His ambition was to invent quaternion analysis which could be as powerful as complex analysis. Unfortunately, this was not successful because of the noncommutative nature of quaternions. Nevertheless, Fueter found the analogy to the Cauchy–Riemann condition for quaternion analysis [1,31]. Consider a quaternionically valued function $f(x, y, z, u)$: It is quaternionic analytic if it satisfies the following Cauchy–Riemann–Fueter condition,

$$\frac{\partial f}{\partial x} + i\frac{\partial f}{\partial y} + j\frac{\partial f}{\partial z} + k\frac{\partial f}{\partial u} = 0. \tag{4.14}$$

Equation (4.14) is the left-analyticity condition since imaginary units are multiplied from the left. A right-analyticity condition can also be similarly defined in which imaginary units are multiplied from the right. The left one is employed throughout this chapter for consistency. For a quaternionic analytic function, the analogy to the Cauchy integral is

$$\frac{1}{2\pi^2}\oiiint \frac{1}{|q-q_0|^2(q-q_0)} Dqf(q) = f(q_0), \tag{4.15}$$

where the integral is over a closed three-dimensional volume surrounding q_0. The measure of the volume element is

$$D(q) = dy \wedge dz \wedge du - idx \wedge dz \wedge du + jdx \wedge dy \wedge du - kdx \wedge dy \wedge dz \tag{4.16}$$

and $K(q)$ is the four-dimensional Green's function,

$$K(q) = \frac{1}{q|q|^2} = \frac{x - yi - zj - uk}{(x^2 + y^2 + z^2 + u^2)^2}. \tag{4.17}$$

There have also been considerable efforts in formulating quantum mechanics and quantum field theory based on quaternions instead of complex numbers [2, 3]. Quaternions are also used to construct the Laughlin-like wavefunctions of the 2D fractional quantum Hall states [32].

As discussed in "*Selected Papers* (1945–1980) *of Chen Ning Yang with Commentary*" [4], C. N. Yang speculated that quaternion quantum theory would be a major revolution to physics, mostly based on the viewpoint of non-Abelian gauge theory. He wrote, "... *I continue to believe that the basic direction is right. There must be an explanation for the existence of* SU(2) *symmetry: Nature, we have repeatedly learned, does not do random things at the fundamental level. Furthermore, the explanation is most likely in quaternion algebra: its symmetry is exactly* SU(2). *Besides, the quaternion algebra is a beautiful structure. Yes, it is noncommutative. But we have already learned that nature chose noncommutative algebra as the language of quantum mechanics. How could she resist using the only other possible nice algebra as the language to start all the complex symmetries that she built into the universe?*"

4.3 Complex analyticity and two-dimensional Landau levels

In this section, I recapitulate the basic knowledge of the 2D Landau-level problem, including the Landau levels of both the nonrelativistic Schrödinger equation in Sec. 4.3.1 and the Dirac equation in Sec. 4.3.2. I explain the complex analyticity of the 2D lowest Landau-level wavefunctions.

4.3.1 *2D Landau levels for nonrelativistic electrons*

Why are the 2D Landau-level wavefunctions so interesting? The answer is their elegancy. The external magnetic field reorganizes the harmonic oscillator wavefunctions to yield analytic properties. To be concrete, the Hamiltonian for a 2D electron moving in an external magnetic field B reads,

$$H_{2D,sym} = \frac{(\vec{P} - \frac{q}{c}\vec{A})^2}{2M}. \tag{4.18}$$

In the symmetric gauge, i.e., $A_x = -\frac{1}{2}By$ and $A_y = \frac{1}{2}Bx$, the 2D rotational symmetry is explicit. The diamagnetic A^2-term corresponds to the harmonic potential, and the cross term becomes the orbital-Zeeman term. Then Eq. (4.18) can be reformulated as

$$H_{2D,sym} = \frac{P_x^2 + P_y^2}{2M} + \frac{1}{2}M\omega_0^2(x^2 + y^2) - \omega_0 L_z, \tag{4.19}$$

where ω_0 is half of the cyclotron frequency ω_c with $\omega_c = qB/(Mc)$ and $qB > 0$ is assumed. Equation (4.19) can be interpreted as the Hamiltonian of a rotating 2D harmonic potential, which is how the Landau-level physics is realized in cold atom systems.

Since the harmonic potential and orbital-Zeeman term commute, the Landau-level wavefunctions are just those of a 2D harmonic oscillator. In Fig. 4.2(a), the spectra of a 2D harmonic oscillator vs. the magnetic quantum number m are plotted, exhibiting a linear dependence on m as $E_{n_r,m} = \hbar\omega_0(2n_r + m + 1)$ where n_r is the radial quantum number. If we view this diagram horizontally, the degeneracies are finite and no nontrivial topology appears. But if they are viewed along the diagonal direction, they become Landau levels. This reorganization is due to the orbital-Zeeman term, which also disperses linearly $E_Z = -m\hbar\omega_0$. It cancels the same linear dispersion of a 2D harmonic oscillator, such that the Landau-level energies are flat. The states with $n_r = 0$ are the lowest Landau-level states, whose wavefunctions are given by

$$\psi_{LLL,m}(z) = z^m e^{-|z|^2/(4l_B^2)}, \tag{4.20}$$

where $m \geq 0$ and the magnetic length $l_B = \sqrt{\hbar c/(qB)}$.

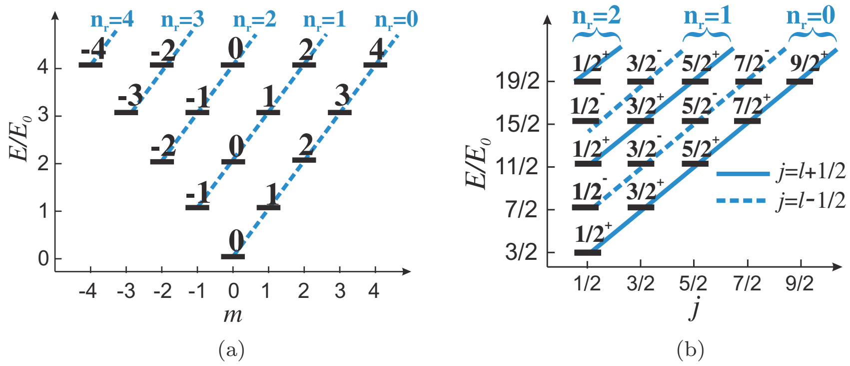

Fig. 4.2. (a) The energy level diagram of a 2D harmonic oscillator vs. the magnetic quantum number m. The states along the tilted lines are reorganized into the 2D flat Landau levels. (b) The eigenstates of a 3D harmonic oscillator labeled by the total angular momentum $j_\pm = l \pm \frac{1}{2}$ Following the tilted solid (dashed) lines, these states are reorganized into the 3D Landau-level states with the positive (negative) helicity for $H^{\pm}_{3D,symm}$, respectively. From Ref. [27].

Now we impose complex analyticity, i.e., the Cauchy–Riemann condition, to select a subset of harmonic oscillator wavefunctions. Physically it is implemented by the magnetic field. It just means that the cyclotron motion is chiral. After suppressing the Gaussian factor, the lowest Landau-level wavefunction is simply as,

$$\psi_{LLL}(z) = f(z), \tag{4.21}$$

which has a one-to-one correspondence to a complex analytic function in the 2D plane. In fact, complex analyticity greatly facilitated the construction of the many-body Laughlin wavefunctions [23],

$$\psi_L(z_1, \ldots, z_n) = \prod_{i<j}(z_i - z_j)^3 e^{-\sum_i \frac{|z_i|^2}{4l_B^2}}, \tag{4.22}$$

which is actually an analytic function of several complex variables.

Along the edge of a 2D Landau-level system, the bulk flat states change to the 1D dispersive chiral edge modes. They satisfy the chiral wave equation [22],

$$\left(\frac{1}{v_f}\frac{\partial}{\partial t} - \frac{\partial}{\partial x}\right)\psi(x,t) = 0, \tag{4.23}$$

where v_f is the Fermi velocity.

4.3.2 *2D Landau levels for Dirac fermions*

This is a square-root problem of the Landau-level Hamiltonian of a Schrödinger fermion in Eq. (4.18). The Hamiltonian reads [33],

$$H_{2D}^D = l_0\omega\{(p_x - A_x)\sigma_x + (p_y - A_y)\sigma_y\}, \tag{4.24}$$

where $A_x = -\frac{1}{2}By$, $A_y = \frac{1}{2}Bx$, $l_0 = \sqrt{\frac{2\hbar c}{|qB|}}$, and $\omega = \frac{|qB|}{2mc}$. It can be recast in the form of

$$H_{2D}^D = \frac{\hbar\omega}{\sqrt{2}}\begin{bmatrix} 0 & a_y^\dagger + ia_x^\dagger \\ a_y - ia_x & 0 \end{bmatrix}, \tag{4.25}$$

where $a_i = \frac{1}{\sqrt{2}}(x_i/l_0 + ip_i l_0/\hbar)$ $(i = x, y)$ are the phonon annihilation operators.

The square of Eq. (4.25) is reduced to the Landau-level Hamiltonian of a Schrödinger fermion with a supersymmetric structure as

$$(H_{2D}^D)^2 \Big/ \left(\frac{1}{2}\hbar\omega\right) = \begin{bmatrix} H_{2D,sym} - \frac{1}{2}\hbar\omega & 0 \\ 0 & H_{2D,sym} + \frac{1}{2}\hbar\omega \end{bmatrix}, \tag{4.26}$$

where $H_{2D,sym}$ is given in Eq. (4.19). The spectra of Eq. (4.25) are $E_{\pm n} = \pm\sqrt{n}\hbar\omega$ where n is the Landau-level index. The zeroth Landau-level states are singled out: Only the upper component of their wavefunctions is nonzero,

$$\Psi^{D}_{2D,LLL}(z) = \begin{pmatrix} \psi_{LLL}(z) \\ 0 \end{pmatrix}. \tag{4.27}$$

Here, $\psi_{LLL}(z)$ is the 2D lowest Landau-level wavefunctions of the Schrödinger equation, which is complex analytic. Other Landau levels with positive and negative energies distribute symmetrically around the zero energy.

Due to the particle–hole symmetry, each state of the zeroth Landau-level is a half-fermion Jackiw–Rebbi mode [29, 34]. When the chemical potential μ approaches $0^{\pm}$, the zeroth Landau-level is fully occupied, or, empty, respectively. The corresponding electromagnetic response is,

$$j_\mu = \pm\frac{1}{8\pi}\frac{q^2}{\hbar}\epsilon_{\mu\nu\lambda}F_{\nu\lambda}, \tag{4.28}$$

which is known as the 2D parity anomaly [33, 35–37]. The signs $\pm$ in Eq. (4.28) refer to $\mu = 0^{\pm}$, respectively. The two spatial components of Eq. (4.28) show the half-quantized quantum Hall conductance, and the temporal component is the half-quantized Streda formula [38].

4.4 3D Landau-level and quaternionic analyticity

We have seen the close connection between complex analyticity and the 2D topological states. In this section, we discuss how to construct high-dimensional topological states in flat spaces based on quaternionic analyticity.

4.4.1 *The 3D Landau-level Hamiltonian*

Our strategy is to construct the 3D Landau levels based on high-dimensional harmonic oscillator wavefunctions. Again we select a subset of them and reorganize them to exhibit nontrivial topological properties: *The selection criterion is quaternionic analyticity, and physically it is a consequence of spin–orbit coupling.* The physical picture of the 3D Landau-level wavefunctions in the symmetric-like gauge is intuitively presented in Fig. 4.3(a), which generalizes the fixed complex plane in the 2D Landau-level problem to a moving frame embedded in 3D. Define a frame with the orthogonal axes $\hat{e}_1$, $\hat{e}_2$, and $\hat{e}_3$, and the complex analytic wavefunctions are defined in

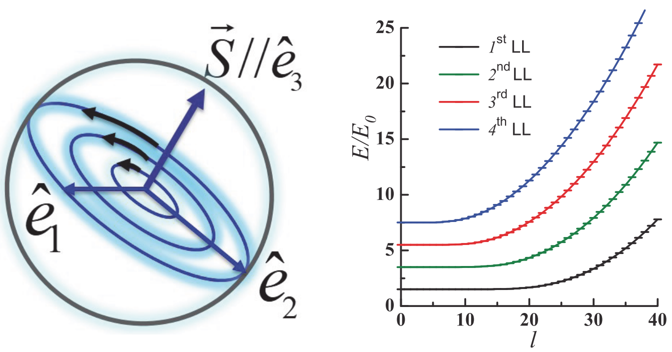

(a) (b)

Fig. 4.3. (a) The coherent state picture for the 3D lowest Landau-level wavefunctions based on Eq. (4.31). $\hat{e}_1$–$\hat{e}_2$–$\hat{e}_3$ form an orthogonal triad. The lowest Landau-level wavefunction is complex analytic in the orbital plane $\hat{e}_1$–$\hat{e}_2$ with spin polarized along $\hat{e}_3$. (b) The surface spectra for the 3D Landau-level Hamiltonian equation (4.29). The open boundary condition is imposed for a ball with the radius $R_0/l_{so} = 8$. From Ref. [27].

the $\hat{e}_1$–$\hat{e}_2$ plane with spin polarized along the $\hat{e}_3$-direction. Certainly this frame can be rotated to an arbitrary configuration. The same strategy can be applied to any high dimensions.

Now we present the 3D Landau-level Hamiltonian as constructed in [27]. Consider coupling a spin-$\frac{1}{2}$ fermion to the 3D isotropic SU(2) Aharonov–Casher potential $\vec{A} = \frac{G}{2}\vec{\sigma} \times \vec{r}$ where G is the coupling constant and $\vec{\sigma}$'s are the Pauli matrices. The resultant Hamiltonian is

$$\begin{aligned} H^{\pm}_{3D,sym} &= \frac{1}{2M}\left(\vec{P} - \frac{q}{c}\vec{A}(\vec{r})\right)^2 + V(\vec{r}) \\ &= \frac{P^2}{2M} + \frac{1}{2}M\omega_0^2 r^2 \mp \omega_0 \vec{\sigma} \cdot \vec{L}, \end{aligned} \tag{4.29}$$

where $\pm$ refer to $G > 0(<0)$, respectively; $\omega_0 = \frac{1}{2}\omega_{so}$ and $\omega_{so} = |qG|/(Mc)$ is the analogy of the cyclotron frequency. $V(r) = -\frac{1}{2}M\omega_0^2 r^2$, nevertheless, the $\frac{1}{2M}(\frac{q}{c})^2 A^2(r)$ term in the kinetic energy contributes a quadratic scalar potential which equals $2|V(r)|$, hence, Eq. (4.29) is still bound from below. In contrast to the 2D case, $H^{\pm}_{3D,sym}$ preserve time-reversal symmetry. It can also be formulated as a 3D harmonic potential plus a spin–orbit coupling term. Again since these two terms commute, the 3D Landau-level wavefunctions are just the eigenstates of a 3D harmonic oscillator.

Consider the eigenstates of a 3D harmonic oscillator with an additional spin degeneracy $\uparrow$ and $\downarrow$. For later convenience, their eigenstates are organized into the eigenbases of the total angular momentum $j_\pm = l \pm \frac{1}{2}$, where $\pm$ represent the positive and negative helicities, respectively. The corresponding spectra are plotted in Fig. 4.2(b), showing a linear dispersion with respect to l as $E_{n_r,J_\pm=l\pm\frac{1}{2},J_z} = \hbar\omega_0\left(2n_r + l + \frac{3}{2}\right)$.

Again, if we view the spectra along the diagonal direction, the novel topology appears. The spin–orbit coupling term $\vec{\sigma}\cdot\vec{L}$ has two branches of eigenvalues, both of which disperse linearly as $l\hbar$ and $-(l+1)\hbar$ for the positive and negative helicity sectors, respectively. Combining the harmonic potential and spin–orbit coupling, we arrive at the flat Landau levels: For H_{3D}^{+}, the positive helicity states become dispersionless with respect to j_+, a main feature of Landau levels. Similarly, the negative helicity states become flat for H_{3D}^{-}. States in the 3D Landau levels exhibit the same helicity.

4.4.2 *The SU(2) group manifold for the lowest Landau-level wavefunctions*

Having understood why the spectra are flat, now we provide an intuitive picture for the lowest Landau-level wavefunctions with the positive helicity. If expressed in the orthonormal basis of (j_+, j_z), they are rather complicated,

$$\psi_{LLL,j_+=l+\frac{1}{2},j_z}(r,\hat{\Omega}) = r^l Y_{j_+=l+\frac{1}{2},j_z}(\hat{\Omega})e^{-\frac{r^2}{4l_{so}^2}}, \tag{4.30}$$

where $l_{so} = \sqrt{\hbar c/|qG|}$ is the analogy of the magnetic length and $Y_{j_+=l+\frac{1}{2},j_z}(\hat{\Omega})$ is the spin–orbit coupled spherical harmonic function with the positive helicity.

Instead, they become very intuitive in the coherent state representation. Let us start with the highest weight states with $j_+ = j_z$, whose wavefunctions are $\psi_{LLL,j_+=j_z}(r,\hat{\Omega}) = (x+iy)^l \exp\{-\frac{r^2}{4l_{so}^2}\}\otimes|\uparrow\rangle$. Their spins are polarized along the z-direction and the orbital channel wavefunctions are complex analytic in the xy plane. We then perform a general SU(2) rotation such that the xyz-frame is rotated to the frame of $\hat{e}_1$–$\hat{e}_2$–$\hat{e}_3$. For a coordinate vector $\vec{r}$, its projection in the $\hat{e}_1$–$\hat{e}_2$-plane forms a complex variable $\vec{r}\cdot(\hat{e}_1 + i\hat{e}_2)$ based on in which plane we construct complex analytic functions.

Now it is clear why spin–orbit coupling is essential. Otherwise, if the orbital plane $\hat{e}_1$–$\hat{e}_2$ is flipped, then the complex variable changes to its conjugate, and the complex analyticity is lost. Nevertheless, the spin is polarized perpendicular along the $\hat{e}_3$, which also flips during the flipping of the orbital plane, such that the helicity remains invariant. In general, we can perform an arbitrary SU(2) rotation on the highest weight states and arrive at a set of coherent states forming the over-complete bases of the lowest Landau-level states as

$$\psi_{LLL,\hat{e}_{1,2,3},j_+}(r,\hat{\Omega}) = [(\hat{e}_1 + i\hat{e}_2)\cdot\vec{r}]^l e^{-\frac{r^2}{4l_{so}^2}} \otimes |\alpha_{\hat{e}_3}\rangle, \quad (l \geq 0), \tag{4.31}$$

where $(\hat{e}_3 \cdot \vec{\sigma})|\alpha_{\hat{e}_3}\rangle = |\alpha_{\hat{e}_3}\rangle$.

Now we can make comparisons among harmonic oscillator wavefunctions in different dimensions:

(1) In 1D, there are only real Hermite polynomials.
(2) In 2D, a subset of harmonic wavefunctions z^m (lowest Landau-level) are selected exhibiting the $U(1)$ structure.
(3) In 3D, define a moving frame $\hat{e}_1$–$\hat{e}_2$–$\hat{e}_3$, which is the same as the rigid-body configuration. The complex plane is $\hat{e}_1$–$\hat{e}_2$. In other words, the configuration space of the 3D lowest Landau-level states is that of a triad, or, the SU(2) group manifold.

Since the SU(2) group manifold is isomorphic to the space of unit quaternions, this motivates us to consider the analytic structure in terms of quaternions, which will be presented in Sec. 4.4.4.

4.4.3 *The off-centered solutions to the lowest Landau-level states*

Different from the 2D Landau-level Hamiltonian, which possesses the magnetic translation symmetry, the 3D Landau-level Hamiltonian equation (4.29) does not possess such a symmetry due to the non-Abelian nature of the SU(2) gauge potential. Nevertheless, based on the coherent state representation described by Eq. (4.31), we can define magnetic translations within the $\hat{e}_1$–$\hat{e}_2$-plane, and organize the off-centered solutions in the 3D lowest Landau-level.

Consider all the coherent states in the $\hat{e}_1$–$\hat{e}_2$-plane described by Eq. (4.31). We define the magnetic translation for this set of states as

$$T_{\hat{e}_3}(\vec{\delta}) = \exp\left(-\vec{\delta}\cdot\vec{\nabla} + \frac{i}{4l_{so}^2}\vec{r}_{12}\cdot(\hat{e}_3\times\vec{\delta})\right), \tag{4.32}$$

where the translation vector $\vec{\delta}$ lies in the $\hat{e}_{1,2}$-plane and $\vec{r}_{12} = \vec{r} - \hat{e}_3(\vec{r}\cdot\hat{e}_3)$. Set $\hat{e}_1 = \hat{z}$, and the normal vector $\hat{e}_3$ lying in the xy-plane with an azimuthal angle ϕ', i.e., $\hat{e}_3(\phi') = \hat{x}\cos\phi' + \hat{y}\sin\phi'$, then $\alpha_{\hat{e}_3}(\phi') = \frac{1}{\sqrt{2}}(|\uparrow\rangle + e^{i\phi'}|\downarrow\rangle)$.

Consider the lowest Landau-level states localized at the origin,

$$\psi_{l=0,\hat{e}_3}(r,\hat{\Omega}) = e^{-\frac{r^2}{4l_{so}^2}} \otimes |\alpha_{\hat{e}_3}\rangle, \tag{4.33}$$

and translate it along $\hat{z}$ at the distance R. According to Eq. (4.32), we arrive at

$$\psi_{\phi',R}(\rho,\phi,z) = e^{i\frac{1}{2l_{so}^2}R\rho\sin(\phi-\phi')} e^{-|\vec{r}-R\hat{z}|^2/4l_{so}^2} \otimes \alpha_{\hat{e}_3}(\phi'), \tag{4.34}$$

where $\rho = \sqrt{x^2+y^2}$ and ϕ is the azimuthal angular of $\vec{r}$ in the xy-plane.

We can restore the rotational symmetry around the $\hat{z}$-axis by performing the Fourier transform with respect to the angle ϕ', i.e., $\psi_{j_z=m+\frac{1}{2},R}(\rho,\phi,z) = \int_0^{2\pi} \frac{d\phi'}{2\pi} e^{im\phi'} \psi_{\phi',R}$. Then the resultant off-centered lowest Landau-level states are the eigenstates of j_z as

$$\psi_{j_z=m+\frac{1}{2},R}(\rho,\phi,z) = e^{\frac{-|\vec{r}-R\hat{z}|^2}{4l_{so}^2}} e^{im\phi}\{J_m(x)|\uparrow\rangle + J_{m+1}(x)e^{i\phi}|\downarrow\rangle\}, \tag{4.35}$$

where $x = R\rho/(2l_{so}^2)$. It describes a wavefunction with the shape of an ellipsoid, whose distribution in the xy-plane is within the distance of ml_{so}^2/R. The states $\psi_{\pm\frac{1}{2},R}$ have the narrowest waist sizes, and their aspect ratio scales as l_{so}/R as R goes large. On the other hand, for those states with $|m| < R/l_{so}$, they localize within the distance of l_{so} from the center located at $R\hat{z}$. As a result, the real space local density of states of the lowest Landau-level grows linearly with R.

4.4.4 *Quaternionic analyticity of the lowest Landau level wavefunctions*

In analogy to complex analyticity of the 2D lowest Landau-level states, we proved that the helicity structure of the 3D lowest Landau levels leads to quaternionic analyticity.

Just like two real numbers forming a complex number, a two-component complex spinor $\psi = (\psi_\uparrow, \psi_\downarrow)^T$ can be mapped to a quaternion by multiplying a j to the second component,

$$f = \psi_\uparrow + j\psi_\downarrow. \tag{4.36}$$

Then, the familiar symmetry transformations can be represented via multiplying quaternions. The time-reversal transformation $i\sigma_2\psi^*$ becomes $Tf = -fj$ satisfying $T^2 = -1$. The $U(1)$ phase $e^{i\theta} \to fe^{i\theta}$, and the SU(2) rotation becomes

$$e^{i\frac{\phi}{2}\sigma_x}\psi \to e^{k\frac{\phi}{2}}f, \quad e^{i\frac{\phi}{2}\sigma_y}\psi \to e^{j\frac{\phi}{2}}f, \quad e^{i\frac{\phi}{2}\sigma_z}\psi \to e^{-i\frac{\phi}{2}}f. \tag{4.37}$$

To apply the Cauchy–Reman–Fueter condition Eq. (4.14) to 3D, we simply suppress the fourth coordinate,

$$\frac{\partial f}{\partial x} + i\frac{\partial f}{\partial y} + j\frac{\partial f}{\partial z} = 0. \tag{4.38}$$

We prove a remarkable property below that this condition (Eq. (4.38)) is rotationally invariant.

Lemma 4.1. *If a quaternionic wavefunction $f(x, y, z)$ is quaternionic analytic, i.e., it satisfies the Cauchy–Riemann–Fueter condition, then after an arbitrary $SU(2)$ rotation, the consequential wavefunction $f'(x, y, z)$ remains quaternionic analytic.*

Proof. Consider an arbitrary SU(2) rotation $g(\alpha, \beta, \gamma) = e^{-i\frac{\alpha}{2}\sigma_z}e^{-i\frac{\beta}{2}\sigma_y}e^{-i\frac{\gamma}{2}\sigma_z}$, where α, β, γ are Euler angles. In the quaternion representation, it maps to $g = e^{i\frac{\alpha}{2}}e^{-j\frac{\beta}{2}}e^{i\frac{\gamma}{2}}$. After this rotation $f(x, y, z)$ transforms to

$$f'(x, y, z) = e^{i\frac{\alpha}{2}}e^{-j\frac{\beta}{2}}e^{i\frac{\gamma}{2}}f(x', y', z'), \tag{4.39}$$

where (x', y', z') are the coordinates by applying g^{-1} on (x, y, z). It can be checked that

$$\left(\frac{\partial}{\partial x} + i\frac{\partial}{\partial y} + j\frac{\partial}{\partial z}\right)e^{i\frac{\alpha}{2}}e^{-j\frac{\beta}{2}}e^{i\frac{\gamma}{2}} = e^{i\frac{\alpha}{2}}e^{-j\frac{\beta}{2}}e^{i\frac{\gamma}{2}}\left(\frac{\partial}{\partial x'} + i\frac{\partial}{\partial y'} + j\frac{\partial}{\partial z'}\right). \tag{4.40}$$

Then we have

$$\left(\frac{\partial}{\partial x} + i\frac{\partial}{\partial y} + j\frac{\partial}{\partial z}\right)f'(x, y, z) = 0. \tag{4.41}$$

Hence, the Cauchy–Riemann–Fueter condition is rotationally invariant. □

Based on this lemma, we prove the quaternionic analyticity of the 3D lowest Landau-level wavefunctions.

Theorem 4.1. *The 3D lowest Landau-level wavefunctions of $H^{+}_{3D,sym}$ in Eq.* (4.29) *have a one-to-one correspondence to the quaternionic analytic polynomials in 3D.*

Proof. We denote the quaternionic polynomials, which correspond to the orthonormal bases of the lowest Landau-level wavefunctions in Eq. (4.30), as $f^{LLL}_{j_+,j_z}$ with $j_+ = l + \frac{1}{2}$, and $-j_+ \leq j_z \leq j_+$. The highest weight states $f^{LLL}_{j_+,j_+} = (x + iy)^l$ are complex analytic in the xy-plane, hence, they are obviously quaternionic analytic. Since all the coherent states can be obtained from the highest weight states via rotations, they are also quaternionic analytic. The coherent states form a set of overcomplex basis of the lowest Landau level wavefunctions, hence all the lowest Landau-level wavefunctions are quaternionic analytic.

Next we prove the completeness that $f^{LLL}_{j_+,j_z}$'s form the complete basis of the quaternionic analytic polynomials in 3D. By counting the degrees of freedom of the lth-order polynomials of x, y, z, and the number of the constraints from Eq. (4.38), we calculate the total number of the linearly independent lth-order quaternionic analytic polynomials as $C^2_{l+2} - C^2_{l+1} = l + 1$. On the other hand, any lowest Landau-level state in the sector of $j_+ = l + \frac{1}{2}$ can be represented as

$$f_l(x, y, z) = \sum_{m=0}^{l} f^{LLL}_{j_+=l+\frac{1}{2},j_z=m+\frac{1}{2}} q_m, \tag{4.42}$$

where q_m is a quaternion constant coefficient. Please note that q_{lm}'s are multiplied from right according to the convention equation (4.36). In Eq. (4.42), we have taken into account the fact $f^{LLL}_{j_+,-j_z} = -f^{LLL}_{j_+,-j_z} j$ due to the time-reversal transformation. Hence, the degrees of freedom in the lowest Landau-level with $j_+ = l+\frac{1}{2}$ are also $l+1$ in the quaternion sense. Hence, the lowest Landau-level wavefunctions are complete for the quaternionic analytic polynomials. □

4.4.5 *Generalizations to 4D and above*

The above procedure can be straightforwardly generalized to four and even higher dimensions. To proceed, we need to employ the Clifford algebra Γ-matrices. Their ranks in different dimensions and concrete representations are presented in Appendix A. Then we employ the N-dimensional (ND) harmonic oscillator potential combined with spin–orbit coupling as

$$H^{ND,LL} = \frac{p^2_{ND}}{2m} + \frac{1}{2} m\omega_0^2 r^2_{ND} - \omega_0 \sum_{1\leq i<j\leq N} \Gamma_{ij} L_{ij}, \tag{4.43}$$

where $L_{ij} = r_i p_j - r_j p_i$. The spectra of Eq. (4.43) were studied in the context of the supersymmetric quantum mechanics [39]. However, its connection with Landau levels was not noticed there. The spin operators in N-dimensions are defined as $\frac{1}{2}\Gamma_{ij}$.

For the 4D case, the minimal representations for the Γ-matrices are still two-dimensional. They are defined as

$$\Gamma_{ij} = -\frac{i}{2}[\sigma_i, \sigma_j], \quad \Gamma_{i4} = \pm\sigma_i, \tag{4.44}$$

with $1 \leq i < j \leq 3$. The $\pm$ signs of Γ^{i4} correspond to two complex conjugate irreducible fundamental spinor representations of SO(4), and the + sign will be taken below. The spectra of the positive helicity states are flat as $E_{+,n_r} = (2n_r + 2)\hbar\omega$. The coherent state picture for the 4D lowest Landau levels can be similarly constructed as follows: Again pick up two orthogonal axes $\hat{e}$ and $\hat{f}$ to form a 2D complex plane, and define complex analytic functions therein as,

$$(x_a\hat{e}_a + ix_a\hat{f}_a)^l e^{-\frac{r^2}{4l_{so}^2}} \otimes |\alpha_{\hat{e},\hat{f}}\rangle, \tag{4.45}$$

where $|\alpha_{\hat{e},\hat{f}}\rangle$ is the eigenstate of $\Gamma^{\hat{e},\hat{f}} = \hat{e}_a\hat{f}_b\Gamma^{ab}$ satisfying

$$\Gamma^{\hat{e},\hat{f}}|\alpha_{\hat{e},\hat{f}}\rangle = |\alpha_{\hat{e},\hat{f}}\rangle. \tag{4.46}$$

Hence, its spin is locked with its orbital angular momentum in the $\hat{e}$–$\hat{f}$-plane.

Following the similar methods in Sec. 4.4.4, we can prove that the 4D lowest Landau-level wavefunctions for Eq. (4.43) satisfy the 4D Cauchy–Riemann–Fueter condition (4.14), and thus are quaternionic analytic functions. Again it can be proved that they form the complete basis for the quaternionic left-analytic polynomials in 4D.

As for even higher dimensions, quaternions are not defined. Nevertheless, the picture of the complex analytic function defined in the moving frame still applies. If we still work in the spinor representation, we can express the lowest Landau-level wavefunctions as $\psi_{LLL}(x_i) = f_{LLL}(x_i)e^{-\frac{r^2}{2l_0^2}}$, where each component of the spinor f_{LLL} is a polynomial of r_i ($1 \leq i \leq N$). To work out the analytic properties of f_{LLL}, we factorize Eq. (4.43) as

$$H^{ND,LL} = \hbar\omega_0(\Gamma^i a_i^\dagger)(\Gamma^j a_j), \tag{4.47}$$

where a_i is the phonon operator in the ith-dimension defined as $a_i = \frac{1}{\sqrt{2}}\left(\frac{1}{l_0}r_i + i\frac{l_0}{\hbar}p_i\right)$, and $l_0 = \sqrt{\frac{\hbar}{m\omega_0}}$. Then $f_{LLL}(x_i)$ satisfies the following equation,

$$\Gamma^j \frac{\partial}{\partial x_j} f_{LLL}(x_i) = 0, \tag{4.48}$$

which can be viewed as the Euclidean version of the Weyl equation. When coming back to 3D and 4D, and following the mapping of Eq. (4.36), we arrive at quaternionic analyticity.

New let us construct the off-centered solutions to the lowest Landau-level states in 4D. We use $\vec{r}$ to denote a point in the subspace of x_1–x_2–x_3, and $\hat{\Omega}$ as an arbitrary unit vector in it. Set $\hat{e} = \hat{\Omega}$ and $\hat{f} = \hat{e}_4$ (the unit vector along the fourth-axis) in Eq. (4.45). $\alpha_{\hat{\Omega}\hat{e}_4}$ satisfies

$$(\sigma_{i4}\Omega_i)\alpha_{\hat{\Omega}\hat{e}_4} = (\vec{\sigma}\cdot\hat{\Omega})\alpha_{\hat{\Omega}\hat{e}_4} = \alpha_{\hat{\Omega}\hat{e}_4}, \tag{4.49}$$

hence,

$$\alpha_{\hat{\Omega}\hat{e}_4} = \left(\cos\frac{\theta}{2}, \sin\frac{\theta}{2}e^{i\phi}\right)^T, \tag{4.50}$$

where we use the gauge convention that the singularity is located at the south pole. Define the magnetic translation in the $\hat{\Omega}$–$\hat{e}_4$-plane,

$$T_{\hat{\Omega}x_4}(u_0\hat{x}_4) = \exp\left(-u_0\partial_{x_4} - \frac{i}{4l_{so}^2}(\vec{r}\cdot\hat{\Omega})u_0\right), \tag{4.51}$$

which translates along the $\hat{e}_4$-axis at the distance of u_0. Apply this translation to the state of $e^{-r^2/4l_{so}^2}\otimes\alpha_{\hat{\Omega}\hat{e}_4}$, we arrive at the off-center solution

$$\psi_{\Omega,u_0}(\vec{r},x_4) = e^{-\frac{r^2+x_4^2}{4l_{so}^2}}e^{-i\frac{ru_0}{2l_{so}^2}}\otimes\alpha_{\hat{\Omega}\hat{e}_4}. \tag{4.52}$$

Next, we perform the Fourier transform over the direction $\hat{\Omega}$,

$$\psi_{4D;j,j_z}(\vec{r},x_4) = \int d\Omega Y^{-\frac{1}{2}}_{l+\frac{1}{2},m+\frac{1}{2}}(\hat{\Omega})\psi_{\Omega,w_0}(\vec{r},x_4), \tag{4.53}$$

where $j = l+\frac{1}{2}$ and $j_z = m+\frac{1}{2}$. Due to the Berry phase structure of $\alpha_{\hat{\Omega}\hat{e}_4}$ over $\hat{\Omega}$, the monopole spherical harmonic functions, $Y^{-\frac{1}{2}}_{l+\frac{1}{2},m+\frac{1}{2}}(\hat{\Omega})$, are used instead of the regular spherical harmonics. Then Eq. (4.53) possesses the 3D rotational symmetry around the new center $(0,0,0,w_0)$, and is characterized by the 3D angular momentum quantum numbers (j, j_z). The monopole harmonic function $Y^q_{jj_z}(\hat{\Omega})$ here is defined as

$$Y^q_{jj_z}(\hat{\Omega}) = \sqrt{\frac{2j+1}{4\pi}}e^{i(j_z+q)\phi}d^l_{j_z,-q}(\theta), \tag{4.54}$$

where θ and ϕ are the polar and azimuthal angles of $\hat{\Omega}$, and $d^l_{j_z,-q}(\theta) = \langle jj_z|e^{-iJ_y\theta}|j-q\rangle$ is the standard Wigner rotation d-matrix. The gauge choice is consistent with that of Eq. (4.50).

4.4.6 *Boundary helical Dirac and Weyl modes*

The topological nature of the 3D Landau-level states is indicated clearly in the gapless surface spectra. Consider a ball of the radius $R_0 \gg l_{so}$ imposed by the open boundary condition. We have numerically solved the spectrum as shown in Fig. 4.3(b). Inside the bulk, the Landau-level spectrum is flat with respect to $j_+ = l + \frac{1}{2}$. As l increases to large values such that the classic orbital radiuses approach the boundary, the Landau levels become surface states and develop dispersive spectra.

We can derive the effective equation for the surface mode based on Eq. (4.29). Since r is fixed at the boundary, it becomes a rotor equation on the sphere. By linearizing the dispersion at the chemical potential μ, and replacing the angular momentum quantum number l by the operator $\vec{\sigma} \cdot \vec{L}$, we arrive at $H_{sf} = (v_f/R_0)\vec{\sigma} \cdot \vec{L} - \mu$ with v_f the Fermi velocity. This is the helical Dirac equation defined on the boundary sphere. When expanded in the local patch around the north pole $R_0\hat{z}$, we arrive at

$$H_{sf} = \hbar v_f(\vec{k} \times \vec{\sigma}) \cdot \hat{z} - \mu. \tag{4.55}$$

The gapless surface states are robust against time-reversal invariant perturbations if odd numbers of helical Fermi surfaces exist according to the $\mathbb{Z}_2$ criterion [6,7]. Since each fully occupied Landau-level contributes one helical Dirac Fermi surface, the bulk is topologically nontrivial if odd numbers of Landau levels are occupied.

A similar procedure can be applied to the high-dimensional case by imposing the open boundary condition to Eq. (4.43). For example, around the north pole of $r_N = (0, \ldots, R_0)$, the linearized low energy equation for the boundary modes is

$$H_{bd} = \hbar v_f \sum_{i=1}^{D-1} k_i \Gamma^{iN} - \mu. \tag{4.56}$$

On the boundary of the 4D sphere, it becomes the 3D Weyl equation that

$$H_{bd} = \hbar v_f \vec{k} \cdot \vec{\sigma} - \mu. \tag{4.57}$$

4.4.7 *Bulk–boundary correspondences*

We have already studied the bulk and boundary states of 2D, 3D and 4D lowest Landau-level states. They exhibit a series of interesting bulk–boundary correspondences as summarized in Table 4.1. In the 2D case, the bulk wavefunctions in the lowest Landau-level is complex analytic satisfying the Cauchy–Riemann condition. The 1D edge states satisfy the chiral wave

Table 4.1. Bulk–boundary correspondences in the lowest Landau-level (LLL) states in 2D, 3D, and 4D.

	Bulk (Euclidean)	Boundary (Minkowski)
2D LLL	Complex analyticity	1D chiral wave
	$\partial_x f + i\partial_y f = 0$	$\partial_t \psi + \partial_x \psi = 0$
3D LLL	3D quaternionic analyticity	2D helical Dirac mode
	$\partial_x f + i\partial_y f + j\partial_z f = 0$	$\partial_t \psi + \sigma_2 \partial_x \psi - \sigma_1 \partial_y \psi = 0$
4D LLL	Quaternionic analyticity	3D Weyl mode
	$\partial_x f + i\partial_y f + j\partial_z f + k\partial_u f = 0$	$\partial_t \psi + \sigma_1 \partial_x \psi + \sigma_2 \partial_y \psi + \sigma_3 \partial_z \psi = 0$

equation (4.23). It is essentially the Weyl equation, which is of single-component in 1D. It can be viewed as the Minkowski version of the Cauchy–Riemann condition of Eq. (4.4). Or, conversely, the Cauchy–Riemann condition for the bulk wavefunctions can be viewed as the Euclidean version of the Weyl equation.

This correspondence goes in parallel in 3D and 4D lowest Landau-level wavefunctions. Their bulk wavefunctions satisfy the quaternionic analytic conditions, which can be viewed as the Euclidean version of the helical Dirac and Weyl equations, respectively.

4.4.8 *Many-body interacting wavefunctions*

It is natural to further investigate many-body interacting wavefunctions in the lowest Landau levels in 3D and 4D. As is well known that the complex analyticity of the 2D lowest Landau-level wavefunctions results in the elegant from of the 2D Laughlin wavefunction Eq. (4.22), which describes a 2D quantum liquid [22,23]. It is natural to further expect that the quaternionic analyticity of the 3D and 4D lowest Landau levels would work as a guidance in constructing high-dimensional SU(2) invariant quantum liquid. Nevertheless, the major difficulty is that quaternions do not commute. It remains challenging how to use quaternions to represent a many-body wavefunction with the spin degree of freedom.

Nevertheless, we present below the spin-polarized fractional many-body states in 3D and 4D Landau levels. In the 3D case, if the interaction is spin-independent, we expect spontaneous spin polarization at very low fillings due to the flatness of lowest Landau-level states in analogy to the 2D quantum Hall ferromagnetism [22,40–43]. According to Eq. (4.31), fermions concentrate to the highest weight states in the orbital plane $\hat{e}_1$–$\hat{e}_2$ with spin polarized along $\hat{e}_3$, then it is reduced to a 2D quantum Hall-like problem on a membrane floating in the 3D space. Any 2D fractional quantum Hall-like state can be formed under suitable interaction pseudopotentials [25, 44, 45]. For example, the $\nu = \frac{1}{3}$ Laughlin-like state on this membrane is constructed as

$$\Psi_{\frac{1}{3}}(\vec{r}_1, \vec{r}_2, \ldots, \vec{r}_n)_{\sigma_1\sigma_2\cdots\sigma_n} = \prod_{i<j}[(\vec{r}_i - \vec{r}_j)\cdot(\hat{e}_1 + i\hat{e}_2)]^3 \otimes|\alpha_{\hat{e}_3}\rangle_{\sigma_1}|\alpha_{\hat{e}_3}\rangle_{\sigma_2}\cdots|\alpha_{\hat{e}_3}\rangle_{\sigma_n}, \tag{4.58}$$

where $|\alpha_{\hat{e}_3}\rangle$ represents a polarized spin eigenstate along $\hat{e}_3$, and the Gaussian weight is suppressed for simplicity. Such a state breaks rotational symmetry and time-reversal symmetry spontaneously, thus it possesses low energy spin-wave modes. Due to the spin–orbit locked configuration in Eq. (4.31), spin fluctuations couple to the vibrations of the orbital motion plane, thus the metric of the orbital plane becomes dynamic. This is a natural connection to the work of geometrical description in fractional quantum Hall states [46–48].

Let us consider the 4D case, we assume that spin is polarized as the eigenstate $|\uparrow\rangle$ of $\Gamma^{12} = \Gamma^{34} = \sigma_3$. The corresponding spin-polarized lowest Landau-level wavefunctions are expressed as

$$\Psi^{4D}_{LLL,m,n} = (x + iy)^m(z + iu)^n \otimes |\uparrow\rangle, \tag{4.59}$$

with $m, n \geq 0$. If all these spin-polarized lowest Landau-level states with $0 \leq m < N_m$ and $0 \leq n < N_n$ are filled, the many-body wavefunction is a Slater-determinant as

$$\Psi^{4D}(v_1, w_1; \ldots; v_N, w_N) = \det[v_i^\alpha w_i^\beta], \tag{4.60}$$

where the coordinates of the ith particle form two pairs of complex numbers as $v_i = x_i + iy_i$ and $w_i = z_i + iu_i$; α, β and i satisfy $0 \leq \alpha < N_m$, $0 \leq \beta < N_n$ and $1 \leq i \leq N = N_m N_n$. Such a state has a 4D uniform density as $\rho = \frac{1}{4\pi^4 l_G^2}$. A Laughlin-like wavefunction can be written down as $\Psi^{4D}_k = (\Psi^{4D})^k$ whose filling relative to ρ should be $1/k^2$. It would be interesting to further study its electromagnetic responses and fractional topological excitations based on Ψ^{4D}_k. Again such a state spontaneously breaks the rotational symmetry, and the coupled spin and orbital excitations would be interesting.

4.5 Dimensional reductions: 2D and 3D Landau levels with broken parity

In this section, we review another class of isotropic Landau-level-like states with time-reversal symmetry but broken parity in both 2D and 3D. The Hamiltonians are again the harmonic potentials plus spin–orbit couplings, but they are the couplings between spin and linear momentum, not orbital angular momentum [26, 49, 50]. They exhibit topological properties very similar to Landau levels.

An early study of these systems filled with bosons can be found in [51]. The spin–orbit coupled Bose–Einstein condensations (BECs) spontaneously break time-reversal symmetry, and exhibit the skyrmion-type spin textures coexisting with half-quantum vortices, which have been reviewed in [52]. Spin–orbit coupled BECs have become an active research direction of cold-atom physics, as extensively studied in [49, 53–57].

4.5.1 *The 2D parity-broken Landau levels*

We consider the Hamiltonian of the Rashba spin–orbit coupling combined with a 2D harmonic potential as

$$H_{2D,hm} = -\frac{\hbar^2\nabla^2}{2M} + \frac{1}{2}M\omega^2 r^2 - \lambda(-i\hbar\nabla_x\sigma_y + i\hbar\nabla_y\sigma_x), \tag{4.61}$$

where λ is the spin–orbit coupling strength with the unit of velocity. Equation (4.61) possesses the $C_{v\infty}$-symmetry and time-reversal symmetry.

We fill the system with fermions and work on its topological properties. There are two different length scales: The trap length scale is defined as $l_T = \sqrt{\frac{\hbar}{M\omega}}$. If, without the trap, the single particle states $\psi_\pm(\vec{k})$ are eigenstates of the helicity operator $\vec{\sigma}\cdot(\vec{k}\times\hat{z})$ whose eigenvalues are ± 1, their spectra are $\epsilon_\pm(\vec{k}) = \hbar^2(k \mp k_0)^2/(2M)$, respectively. The lowest energy states are $\psi_+(\vec{k})$ located around a ring in momentum space with radius $k_0 = M\lambda/\hbar$. This introduces a spin–orbit length scale as $l_{so} = 1/k_0$. Then the ratio between these two length scales defines a dimensionless parameter $\alpha = l_T/l_{so}$, which describes the spin–orbit coupling strength relative to the harmonic potential.

In the case of strong spin–orbit coupling, i.e., $\alpha \gg 1$, a clear picture appears in momentum space. The low energy states are reorganized from the plane-wave states $\psi_+(\vec{k})$ with $k \approx k_0$. Since $\alpha \gg 1$, we can safely project out the negative helicity states $\psi_-(\vec{k})$ at high-energy, then the harmonic potential in the low energy sector becomes a Laplacian in momentum space subject to a Berry connection $\vec{A}_k$ as

$$V = \frac{M}{2}\omega^2 r^2 = \frac{M}{2}\omega^2(i\nabla_k - A_k)^2, \tag{4.62}$$

which drives the particle moving around the ring. It is well known that for the Rashba Hamiltonian, the Berry connection A_k gives rise to a π-flux at $\vec{k} = (0, 0)$ but zero Berry curvature at $\vec{k} \neq 0$ [58]. The consequence is that the angular momentum eigenvalues become half-integers as $j_z = m + \frac{1}{2}$. The angular dispersion of the spectra can be estimated as $E_{agl}(j_z) = (j_z^2/2\alpha^2)\hbar\omega$, which is strongly suppressed by spin–orbit coupling. On the other hand, the radial energy quantization remains as usual $E_{rad}(n_r) = \left(n_r + \frac{1}{2}\right)\hbar\omega$ up to a constant. Hence the total energy dispersion is

$$E_{n_r,j_z} \approx \left(n_r + \frac{1}{2} + \frac{j_z^2}{2\alpha^2}\right)\hbar\omega. \tag{4.63}$$

Similar results have also been obtained in [53–55]. Since $\alpha \gg 1$, the spectra are nearly flat with respect to j_z, we can treat n_r as a Landau-level index.

Next we define the edge modes of such systems, and their stability problem is quite different from that of the chiral edge modes of 2D magnetic Landau-level systems. In the regime that $\alpha \gg 1$, the spin–orbit length l_{so} is much shorter than l_T, such that l_T is viewed as the cutoff of the sample size. States with $|j_z| < \alpha$ are viewed as bulk states which localize within the region of $r < l_T$. For states with $|j_z| \sim \alpha$, their energies touch the bottom of the next higher Landau-level, and thus they should be considered as edge states. Due to time-reversal symmetry, each filled Landau-level of Eq. (4.61) gives rise to a branch of edge modes of Kramers' doublets $\psi_{n_r,\pm j_z}$. In other words, these edge modes are helical rather than chiral. Similarly to the Z_2 criterion in [6, 7], which was defined for Bloch wave states, in our case the following mixing term, $H_{mx} = \psi^\dagger_{2D,n_r,j_z}\psi_{2D,n_r,-j_z} + h.c.$, is forbidden by time-reversal symmetry. Consequently, the topological index for this system is Z_2.

4.5.2 *Dimensional reduction from 3D Landau levels*

In fact, we construct a Hamiltonian closely related to Eq. (4.61) such that its ground state is solvable exhibiting exactly flat dispersion. It is a consequence of the dimensional reduction based on the 3D Landau-level Hamiltonian equation (4.29). We cut a 2D off-centered plane perpendicular to the z-axis with the interception $z = z_0$. In this off-centered plane, inversion symmetry is broken, and Eq. (4.29) is reduced to

$$H_{2D,re} = H_{2D,hm} - \omega L_z \sigma_z. \tag{4.64}$$

The first term is just Eq. (4.61) by identifying $\lambda = \omega z_0$ and the frequency of the second term is the same as that of the harmonic trap. If $z_0 = 0$, the Rashba spin–orbit coupling vanishes, and Eq. (4.64) becomes the 2D quantum spin-Hall Hamiltonian, which is a double copy of Eq. (4.19). At $z_0 \neq 0$, σ_z is no longer conserved due to spin–orbit coupling.

In Sec. 4.4.3, we derived the off-centered ellipsoid type wavefunction. After setting $z = z_0$ in Eq. (4.35), we arrive at the following 2D wavefunction,

$$\psi_{2D,j_z}(r,\phi) = e^{-\frac{r^2}{4l_{so}^2}}\{e^{im\phi}J_m(k_0r)|\uparrow\rangle + e^{i(m+1)\phi}J_{m+1}(k_0r)|\downarrow\rangle\}, \quad (4.65)$$

where $J_m(k_0r)$ is the mth order Bessel functions. It is straightforward to prove that the simple reduction indeed gives rise to the solutions of the lowest Landau level to Eq. (4.64), since the partial derivative along the z-direction of the solution in Eq. (4.35) equals zero at $z = z_0$. We also prove that the energy dispersion is exactly flat as,

$$H_{2D,re}\psi_{2D,j_z} = \left(1 - \frac{\alpha^2}{2}\right)\hbar\omega\psi_{2D,j_z}. \quad (4.66)$$

The above two Hamiltonians equations (4.64) and (4.61) are nearly the same except the $L_z\sigma_z$ term, whose effect relies on the distance from the origin. Consider the lowest Landau-level solutions at $\alpha \gg 1$. The decay length of the Gaussian factor in Eq. (4.65) is l_T. Nevertheless, the Bessel functions peak around $k_0r_0 \approx m$, i.e., $r_0 \approx \frac{m}{\alpha}l_T$. Hence for states with $j_z < \alpha$, their wavefunctions already decay before reach l_T. Then the $L_z\sigma_z$-term compared to the Rashba one is a small perturbation at the order of $\omega r_0/\lambda = r_0/z_0 \ll 1$. In this regime, these two Hamiltonians are equivalent. In contrast, in the opposite limit that $j_z \gg \alpha^2$, the Bessel functions are cut off by the Gaussian factor, and only their initial power-law parts participate. The classic orbit radii are just $r_0 \approx \sqrt{m}l_T$, then the physics of Eq. (4.64) is controlled by the $L_s\sigma_z$-term as in the quantum spin-Hall systems. For the intermediate region that $\alpha < j_z < \alpha^2$, the physics is a crossover between the above two limits.

The many-body physics based on the above spin–orbit coupled Landau levels in Eq. (4.65) would be very interesting. Fractional topological states would be expected which are both rotationally and time-reversal invariant. However, σ_z is not a good quantum number and parity is also broken, hence, these states should be very different from a double copy of the fractional Laughlin states with spin-up and spin-down particles. The nature of topological excitations and properties of edge modes will be deferred to a future study.

4.5.3 *The 3D parity-broken Landau levels*

We have also considered the problem of a 3D harmonic potential plus a Weyl-type spin–orbit coupling, whose Hamiltonian is defined as [26],

$$H_{3D,hm} = -\frac{\hbar^2\nabla^2}{2M} + \frac{1}{2}M\omega^2r^2 - \lambda(-i\hbar\vec{\nabla}\cdot\vec{\sigma}). \quad (4.67)$$

The analysis can be performed in parallel to the 2D case. In the absence of spin–orbit coupling, the low energy states of Eq. (4.67) in momentum space form a spin–orbit sphere. The harmonic potential further quantizes the energy spectra as

$$E_{n_r,j,j_z} \approx \left(n_r + \frac{1}{2} + \frac{j(j+1)}{2\alpha^2}\right)\hbar\omega, \tag{4.68}$$

where n_r is the Landau-level index and j is the quantum number of the total angular momentum. Again j takes half-integer values because the Berry phase on the low-energy sphere exhibits a unit monopole structure.

Now we perform the dimensional reduction from the Hamiltonian equation (4.43) in the 4D case to 3D. We cut a 3D off-centered hyper-plane perpendicular to the fourth axis with the interception $x_4 = u_0$. Within this 3D hyper-plane of $(x_1, x_2, x_3, x_4 = u_0)$, Eq. (4.43) is reduced to

$$H_{3D,re} = H_{3D,hm} - \omega\vec{L}\cdot\vec{\sigma}, \tag{4.69}$$

where the first term is just Eq. (4.67) with the spin–orbit coupling strength set by $\lambda = \omega u_0$. Again, based on the center-shifted wavefunction in the lowest Landau level equation (4.53), and by setting $x_4 = u_0$, we arrive at the following wavefunction

$$\psi_{3D,JJ_z}(\vec{r}) = e^{-\frac{r^2}{4l_{so}^2}}\{j_l(k_0r)Y_{+,J,J_z}(\Omega_r) + ij_{l+1}(k_0r)Y_{-,J,J_z}(\Omega_r)\}, \tag{4.70}$$

where $k_0 = u_0/l_T^2 = m\lambda/\hbar$; j_l is the lth order spherical Bessel function. $Y_{\pm,j,l,j_z}$'s are the spin–orbit coupled spherical harmonics defined as

$$Y_{+,j,l,j_z}(\Omega) = \left(\sqrt{\frac{l+m+1}{2l+1}}Y_{lm}, \sqrt{\frac{l-m}{2l+1}}Y_{l,m+1}\right)^T$$

with the positive eigenvalue of $l\hbar$ for $\vec{\sigma}\cdot\vec{L}$, and

$$Y_{-,j,l,j_z}(\Omega) = \left(-\sqrt{\frac{l-m}{2l+1}}Y_{lm}, \sqrt{\frac{l+m+1}{2l+1}}Y_{l,m+1}\right)^T$$

with the negative eigenvalue of $-(l+1)\hbar$ for $\vec{\sigma}\cdot\vec{L}$. It is straightforward to check that $\psi_{3D,j,j_z}(\vec{r})$ in Eq. (4.70) is the ground-state wavefunction satisfying

$$H_{3D,re}\psi_{3D,j,j_z}(\vec{r}) = \left(\frac{3}{2} - \frac{\alpha^2}{2}\right)\hbar\omega\psi_{3D,j,j_z}(\vec{r}). \tag{4.71}$$

4.6 High-dimensional Landau levels of Dirac fermions

In this section, we review the progress on the study of 3D Landau levels of relativistic Dirac fermions [28]. This is a square-root problem of the 3D Landau-level problem based on the Schrödinger equation reviewed in Sec. 4.4. This can also be viewed as Landau levels of complex quaternions.

4.6.1 *3D Landau levels for Dirac fermions*

In Eq. (4.25), two sets of phonon creation and annihilation operators $(a_x, a_y; a_x^\dagger, a_y^\dagger)$ are combined with the real and imaginary units to construct the Landau-level Hamiltonian for 2D Dirac fermions. Since in 3D there exist three sets of phonon creation and annihilation operators, complex numbers are insufficient.

The new strategy is to employ the Pauli matrices $\vec{\sigma}$ such that

$$H_{3D}^D = v\left\{\alpha_i p_i + \gamma_i i\hbar \frac{r_i}{l_0^2}\right\} = \frac{\hbar\omega}{\sqrt{2}}\begin{bmatrix} 0 & i\sigma_i a_i^\dagger \\ -i\sigma_i a_i & 0 \end{bmatrix}, \tag{4.72}$$

where the repeated index i runs over x, y and z; $v = \frac{1}{2} l_0 \omega$. The convention of γ-matrices is

$$\beta = \gamma_0 = \tau_3 \otimes I, \quad \alpha_i = \tau_1 \otimes \sigma_i, \quad \gamma_i = \beta\alpha_i = i\tau_2 \otimes \sigma_i. \tag{4.73}$$

Equation (4.72) contains the complex combination of momenta and coordinates, thus it can be viewed as the generalized Dirac equation defined in the phase space. Apparently, Eq. (4.72) is rotationally invariant. It is also time-reversal invariant under the definition $T = \gamma_2\gamma_3 K$ where K is the complex conjugation, and $T^2 = -1$. Since $\beta H_{3D}^D \beta = -H_{3D}^D$, H_{3D}^D possesses the particle–hole symmetry and its spectra are symmetric with respect to the zero energy.

Similar to the 2D case, $(H_{3D}^D)^2$ has a supersymmetric structure. The square of Eq. (4.72) is block-diagonal, and two blocks are just the nonrelativistic 3D Landau-level Hamiltonians in Eq. (4.29),

$$\frac{(H_{3D}^D)^2}{\frac{1}{2}\hbar\omega} = \begin{bmatrix} H_{3D,sym}^+ - \frac{3}{2}\hbar\omega & 0 \\ 0 & H_{3D,sym}^- + \frac{3}{2}\hbar\omega \end{bmatrix}, \tag{4.74}$$

where the mass M in $H_{3D,sym}^\pm$ is defined through the relation $l_0 = \sqrt{\hbar/(M\omega)}$. Based on Eq. (4.74), the energy eigenvalues of Eq. (4.72) are $E_{\pm n_r, j, j_z} = \pm\hbar\omega\sqrt{n_r}$, corresponding to positive and negative square roots of the nonrelativistic dispersion, respectively. The Landau-level wavefunctions of the 3D Dirac electrons are expressed in terms of the nonrelativistic ones of Eq. (4.29) as

$$\Psi_{\pm n_r,j,j_z}(\vec{r}) = \frac{1}{\sqrt{2}} \begin{pmatrix} \psi_{n_r,j_+,l,j_z}(\vec{r}) \\ \pm i\psi_{n_r-1,j_-,l+1,j_z}(\vec{r}) \end{pmatrix}. \tag{4.75}$$

Please note that the upper and lower two components possess different values of orbital angular momenta. They exhibit opposite helicities of $j_\pm$, respectively. The zeroth Landau-level ($n_r = 0$) states are special: There is only one branch, and only the first two components of the wavefunctions are nonzero as

$$\Psi_{n_r=0,j,j_z}(\vec{r}) = \begin{bmatrix} \Psi_{LLL,j_+,j_z}(\vec{r}) \\ 0 \end{bmatrix}, \tag{4.76}$$

where Ψ_{LLL,j_+,j_z}'s are the lowest Landau level solutions to the nonrelativistic Hamiltonian Eq. (4.29).

Again the nontrivial topology of the 3D Dirac Landau problem manifests in the gapless surface modes. Consider a spherical boundary with a large radius R. The Hamiltonian takes the form of Eq. (4.72) inside the sphere, and changes to the usual massive Dirac Hamiltonian $H_D = \alpha_i P_i + \beta\Delta$ outside. We take the limit of $|\Delta| \to \infty$. Loosely speaking, this is a square-root version of the open boundary problem of the 3D nonrelativistic case in Sec. 4.4.6. Since square-roots can be taken as positive and negative, each branch of the surface modes in the nonrelativistic Schrödinger case corresponds to a pair of relativistic surface branches. These two branches disperse upward and downward as increasing the angular momentum j, respectively. However, the zeroth Landau-level branch is singled out. We can only take either the positive or negative square root for its surface excitations. Hence, the surface spectra connected to the bulk zeroth Landau-level disperse upward or downward depending on the sign of the vacuum mass.

4.6.2 *Nonminimal Pauli coupling and anomaly*

Due to the particle–hole symmetry of Eq. (4.72), the 3D zeroth Landau-level states are half-fermion modes in the same way as those in the 2D Dirac case. Moreover, in the 3D case, the degeneracy is over the 3D angular momentum numbers (j_+, j_z), thus the degeneracy is much higher than that of 2D. According to whether the chemical potential μ approaches 0^+ or 0^-, each state in the zeroth lowest Landau level contributes a positive, or, negative half fermion number, respectively. The Lagrangian of the 3D massless Dirac

Landau level problem is,

$$L = \bar{\psi}\{\gamma_0 i\hbar\partial_t - iv\gamma_i\hbar\partial_i\}\psi - v\hbar\bar{\psi}i\gamma_0\gamma_i\psi F^{0i}(r), \tag{4.77}$$

where $F^{0i} = x_i/l_0^2$. In all the dimensions higher than 2, $i\gamma_0\gamma_i$'s are a different set from γ_i's, thus Eq. (4.77) is an example of nonminimal coupling of the Pauli type. More precisely, it is a coupling between the electric field and the electric dipole moment. In the 2D case, the Lagrangian has the same form as Eq. (4.77), however, since $\gamma_{0,1,2}$ are just the usual Pauli matrices, it is reduced to the minimal coupling to the $U(1)$ gauge field.

Equation (4.77) is a problem of massless Dirac fermions coupled to a background field via a nonminimal Pauli coupling at 3D and above. The Fermion density is pumped by the background field from vacuum. This is similar to parity anomaly, and indeed it is reduced to parity anomaly in 2D. However, the standard parity anomaly only exists in even spatial dimensions [33, 35–37]. By contrast, the Landau-level problems of massless Dirac fermions can be constructed in any high spatial dimensions. Obviously, they are not chiral anomalies defined in odd spatial dimensions, either. It would be interesting to further study the nature of such kind of "anomaly".

In fact, Eq. (4.72) is just one possible representation for Landau levels of 3D massless Dirac fermions. A general 3D Dirac Landau-level Hamiltonian with a mass term can be defined as

$$\begin{aligned} H^D_{3D}(\hat{e}_1, \hat{e}_2, \hat{e}_3) = v[(\vec{\tau}\cdot\hat{e}_1)\otimes\sigma_i P_i + \hbar/l_0^2(\vec{\tau}\cdot\hat{e}_2) \\ \otimes\sigma_i r_i] + mv^2(\vec{\tau}\cdot\hat{e}_3)\otimes I, \end{aligned} \tag{4.78}$$

where $\tau_{1,2,3}$ are Pauli matrices acting in the particle–hole channel, and $\hat{e}_{1,2,3}$ form an orthogonal triad in the 3D space. Equation (4.72) corresponds to the case of $\hat{e}_1 = \hat{x}$ and $\hat{e}_2 = \hat{y}$, and $m = 0$. The parameter space of $H^D_{3D}(\hat{e}_1, \hat{e}_2, \hat{e}_3)$ is the triad configuration space of SO(3).

Consider that the configuration of the triad $\hat{e}_{1,2,3}$ is spatially dependent. The first term in Eq. (4.78) should be symmetrized as $\frac{1}{2}\vec{\tau}\cdot[(\hat{e}_1(r)P_i + P_i\hat{e}_1(r)]\otimes\sigma_i$. The spatial distribution of the triad of $\hat{e}_{1,2,3}(\vec{r})$ can be in a topologically nontrivial configuration. If the triad is only allowed to rotate around a fixed axis, its configuration space is $U(1)$ which can form a vortex line type defect. There should be a Callan–Harvey type effect of the fermion zero modes confined around the vortex line [59]. In general, we can also have a 3D skyrmion type defect of the triad configuration. These novel defect problems and the associated zero energy fermionic excitations will be deferred to later studies.

4.6.3 *Landau levels for Dirac fermions in four dimensions and above*

The Landau-level Hamiltonian for Dirac fermions can be generalized to arbitrary N-dimensions (ND) by replacing the Pauli matrices in Eq. (4.72) with the Clifford algebra Γ-matrices in ND. We use the representation of the Γ-matrices as presented in Appendix A.

In odd dimensions $D = 2k + 1$, we use the kth rank Γ-matrices to construct the $D = 2k + 1$-dimensional Dirac Landau-level Hamiltonian,

$$H^D_{2k+1} = \frac{\hbar\omega_0}{2}\begin{pmatrix} 0 & i\Gamma^{(k)}_i a^\dagger_i \\ -i\Gamma^{(k)}_i a_i & 0 \end{pmatrix}, \tag{4.79}$$

where $\Gamma^{(k)}_i$ is $2^k \times 2^k$-dimensional matrix, and $1 \le i \le 2k+1$. Again, $(H^D_{2k+1})^2$ are reduced to a supersymmetric version of the $2k + 1$-dimensional Landau-level Hamiltonian for Schödinger fermions in Eq. (4.43). All other properties are parallel to the 3D case explained before.

For even dimensions $D = 2k$, we still take Eq. (4.79) by simply removing the terms of the $(2k + 1)$th dimension and keeping the terms from the first to the $(2k)$th dimension. Nevertheless, such a construction is reducible. In the representation presented in Appendix A, Eq. (4.79) after eliminating the $\Gamma^{(k)}_{2k+1}$ term can be factorized into a pair of Hamiltonians

$$H^{\pm,D}_{2k} = \frac{\hbar\omega_0}{2}\begin{pmatrix} 0 & \pm a^\dagger_{2k} + i\sum_{i=1}^k \Gamma^{(k-1)}_i a^\dagger_i \\ \pm a_k - i\sum_{i=1}^k \Gamma^{(k-1)}_i a_i & 0 \end{pmatrix}, \tag{4.80}$$

where $\pm$ correspond to the pair of fundamental and anti-fundamental spinor representations in even dimensions.

For example, in four dimensions, we have

$$H^{\pm,D}_{4D} = \frac{\hbar\omega}{\sqrt{2}}\begin{bmatrix} 0 & \pm a^\dagger_4 + i\sigma_i a^\dagger_i \\ \pm a_4 - i\sigma_i a_i & 0 \end{bmatrix}. \tag{4.81}$$

Since three quaternionic imaginary units i, j, and k can be mapped to Pauli matrices $-i\sigma_1, -i\sigma_2$, and $-i\sigma_3$, respectively, and the annihilation and creation operators are essentially complex. $\pm a_4 - i\sigma_i a_i$ can be viewed as complex quaternions. Hence, Eq. (4.81) is a complex quaternionic generalization of the 2D Dirac Landau-level Hamiltonian equation (4.25).

4.7 High-dimensional Landau levels in the Landau-like gauge

We have discussed the construction of Landau levels in high dimensions for both Schrödinger and Dirac fermions in the symmetric-like gauge. In these problems, the rotational symmetry is explicitly maintained. Below we review the construction of Landau levels in the Landau-like gauge by reorganizing plane-waves to exhibit nontrivial topological properties [30]. It still preserves the flat spectra but not the rotational symmetry.

4.7.1 *Spatially separated 1D chiral modes: 2D Landau levels*

We recapitulate the Landau levels in the Landau gauge. By setting $A_x = By$ and $A_y = 0$ in the Hamiltonian equation (4.18), we arrive at

$$H_{2D,L} = \frac{P_y^2}{2M} + \frac{\left(P_x - \frac{e}{c}A_x\right)^2}{2M} = \frac{P_y^2}{2M} + \frac{1}{2}M\omega^2(y - l_B^2 P_x)^2, \tag{4.82}$$

with $l_B = \sqrt{\frac{\hbar}{M\omega}}$. The Landau-level wavefunctions are a product of a plane wave along the x-direction and a 1D harmonic oscillator wavefunction in the y-direction,

$$\psi_n(x, y) = e^{ik_x}\phi_n(y - y_0(k)), \tag{4.83}$$

where ϕ_n is the nth harmonic oscillator eigenstate with the characteristic length l_B, and its equilibrium position is determined by the momentum k_x, $y_0(k_x) = l_B^2 k_x$.

Hence, the Landau-level states with positive and negative values of k_x are shifted oppositely along the y-direction, and become spatially separated. If imposing the open boundary condition along the y-axis, chiral edge modes appear. The 2D quantum Hall effect is just the spatially separated 1D chiral anomaly in which the chiral current becomes the transverse charge current. After the projection to the lowest Landau level, we identify $y = l_B^2 k_x$, hence, the two spatial coordinates x and y become noncommutative as [60]

$$[x, y]_{LLL} = i l_B^2. \tag{4.84}$$

In other words, the xy-plane is equivalent to the 2D phase space of a 1D system $(x; k_x)$ after the lowest Landau-level projection.

4.7.2 *Spatially separated 2D helical modes: 3D Landau levels*

The above picture can be generalized to the 3D Landau-level states: We keep the plane-wave modes with the good momentum numbers (k_x, k_y) and shift them along the z-axis. Spin–orbit coupling is introduced to generate the helical structure to these plane-waves, and the shifting direction is determined by the sign of helicity. To be concrete, the 3D Landau-level Hamiltonian in the Landau-like gauge is constructed as follows [30],

$$\begin{aligned} H^{\pm}_{3D,L} &= \frac{\vec{P}^2}{2M} + \frac{1}{2}M\omega_{so}^2 z^2 \mp \omega_{so} z(P_x\sigma_y - P_y\sigma_x) \\ &= \frac{P_z^2}{2M} + \frac{1}{2}M\omega_{so}^2\left[z \mp \frac{1}{\hbar} l_{so}^2 (P_x\sigma_y - P_y\sigma_x)\right]^2, \end{aligned} \tag{4.85}$$

where $l_{so} = \sqrt{\hbar/(M\omega_{so})}$.

The key of Eq. (4.85) is the z-dependent Rashba spin–orbit coupling, such that it can be decomposed into a set of 1D harmonic oscillators along the z-axis coupled to 2D helical plane-waves. Define the helicity operator $\hat{\Sigma}_{2d}(\hat{k}_{2d}) = \hat{k}_x\sigma_y - \hat{k}_y\sigma_x$ where $\hat{k}$ is the unit vector along the direction of $\vec{k}$. $\chi_\Sigma(\hat{k}_{2d})$ is the eigenstate of $\hat{\Sigma}$ and $\Sigma = \pm 1$ is the eigenvalue. Then the 3D Landau-level wavefunctions are expressed as

$$\Psi_{n,\vec{k}_{2d},\Sigma}(\vec{r}) = e^{i\vec{k}_{2d}\cdot\vec{r}_{2d}}\phi_n[z - z_0(k_{2d},\Sigma)] \otimes \chi_\Sigma(\hat{k}_{2d}), \tag{4.86}$$

where $\vec{k}_{2d} = (k_x, k_y)$, $\vec{r}_{2d} = (x, y)$, and $k_{2d} = (k_x^2 + k_y^2)^{\frac{1}{2}}$. The energy spectra of Eq. (4.86) is flat as $E_n = (n + \frac{1}{2})\hbar\omega_{so}$. The center of the oscillator wavefunction in Eq. (4.86) is shifted to $z_0 = l_{so}^2 k_{2d}\Sigma$.

The 3D Landau-level wavefunctions of Eq. (4.86) are spatially separated 2D helical plane-waves along the z-axis. As shown in Fig. 4.4(a), for states with opposite helicity eigenvalues, their central positions are shifted in opposite directions. If open boundaries are imposed perpendicular to the z-axis, each Landau level contributes a branch of gapless helical Dirac modes. For the system described by $H^{+}_{3D,L}$, the surface Hamiltonian is

$$H_{bd} = \pm v_f(\vec{p} \times \vec{\sigma}) \cdot \hat{z} - \mu, \tag{4.87}$$

where $\pm$ apply to the upper and lower boundaries, respectively.

Unlike the 2D case in which the symmetric and Landau gauges are equivalent, the Hamiltonian in the symmetric-like gauge equation (4.29) and that in the Landau-like gauge equation (4.85) are *not* gauge equivalent. The Landau-like gauge explicitly breaks the 3D rotational symmetry while the symmetric-like gauge preserves it. Physical quantities calculated based on Eq. (4.85), such as density of states, are not 3D rotationally symmetric as those based on Eq. (4.29). Nevertheless, these two Hamiltonians belong to the same topological class.

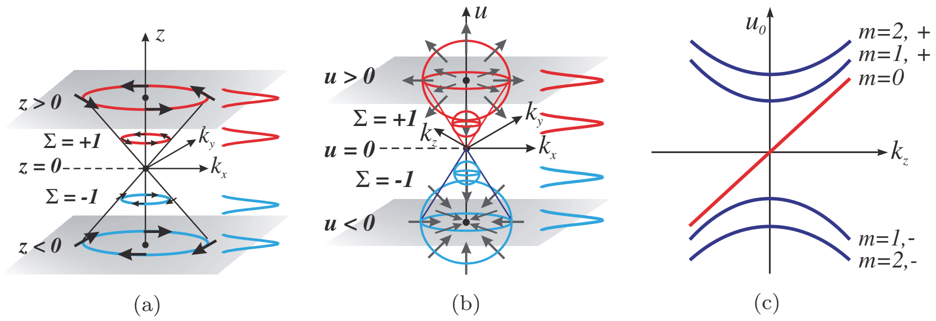

Fig. 4.4. (a) 3D Landau-level wavefunctions as spatially separated 2D helical Dirac modes localized along the z-axis. (b) 4D Landau-level wavefunctions as spatially separated 3D Weyl modes localized along the u-axis. Note that 2D plane-wave modes with opposite helicities and the 3D ones with opposite chiralities are located at opposite sides of $z = 0$ and $u = 0$ planes, respectively. (c) The central positions $u_0(m, k_z, \nu)$ of the 4d Landau levels in the presence of the magnetic field $\vec{B} = B\hat{z}$. The branch of $m = 0$ runs across the entire u-axis, which gives rise to the quantized charge transport along the u-axis in the presence of $\vec{E} \parallel \vec{B}$ as indicated in Eq. (4.43). From Ref. [30].

4.7.3 *Spatially separated 3D Weyl modes: 4D Landau levels*

Again we can easily generalize the above procedure to any dimensions. For example, in four dimensions, we need to use the 3d helicity operator $\hat{\Sigma}_{3d} = \hat{P}_{3d} \cdot \vec{\sigma}$, whose eigenstates are denoted as χ_Σ with the eigenvalues $\Sigma = \pm 1$. Then the 4D Landau-level Hamiltonian is defined as [30]

$$\begin{aligned} H_{LL}^{4d,\pm} &= \frac{P_u^2 + \vec{P}_{3d}^2}{2M} + \frac{1}{2} M\omega^2 u^2 \mp \omega u \vec{P}_{3d} \cdot \vec{\sigma} \\ &= \frac{P_u^2}{2M} + \frac{1}{2} M\omega_{so}^2 \left(u \mp \frac{1}{\hbar} l_{so}^2 \vec{P}_{3d} \cdot \vec{\sigma} \right)^2, \end{aligned} \tag{4.88}$$

where u and P_u are the coordinate and momentum in the fourth dimension, respectively, and $\vec{P}_{3d}$ is defined in the xyz-space. Inside each Landau level, the spectra are flat with respect to $\vec{k}_{3d}$ and Σ. Similarly to the 3D case, the 4D LL spectra and wavefunctions are solved by reducing Eq. (4.88) into a set of 1D harmonic oscillators along the u-axis as

$$\Psi_{n,\vec{k}_{3d},\Sigma}(\vec{r}, u) = e^{i\vec{k}_{3d}\cdot\vec{r}} \phi_n[u - u_0(k_{3d}, \Sigma)] \otimes \chi_\Sigma(\vec{k}_{3d}). \tag{4.89}$$

The central positions $u_0(k_{3d}, \Sigma) = \Sigma l_{so}^2 k_{3d}$. This realizes the spatial separation of the 3D Weyl fermion modes with the opposite chiralities as shown in Fig. 4.4(b). With an open boundary imposed along the u-direction, the 3D chiral Weyl fermion modes appear on the boundary

$$H_{bd} = \pm v_f (\vec{k}_{3D} \cdot \vec{\sigma}) - \mu. \tag{4.90}$$

4.7.4 *Phase space picture of high-dimensional Landau levels*

For the 2D case described by Eq. (4.82), the xy-plane is equivalent to the 2D phase space of a 1D system $(x; k_x)$ after the lowest Landau-level projection. The discrete step of k_x is $\Delta k_x = 2\pi/L_x$, and the momentum cutoff of the bulk state is determined by L_y as $k_{bk} = L_y/(2l_B^2)$. Since $|k_x| < k_{bk}$, the number of states $N_{2D,LL}$ scales with $L_x L_y$ as the usual 2D systems, but the crucial difference is that enlarging L_y does not change Δk_x but instead increases k_{bk}.

Similarly, the 3D Landau-level states (Eq. (4.85)) can be viewed as states in the 4D phase space $(xy; k_x k_y)$. The z-axis plays the double role of k_x and k_y. After the lowest Landau-level projection, z is equivalent to $z = l_{so}^2(p_x\sigma_y - p_y\sigma_x)/\hbar$, and thus

$$[x, z]_{LLL} = il_{so}^2\sigma_y, \quad [y, z]_{LLL} = -il_{so}^2\sigma_x, \quad [x, y]_{LLL} = 0. \tag{4.91}$$

The momentum cutoff of the bulk state is determined as $(k_x^2 + k_y^2)^{\frac{1}{2}} < k_{bk} = \hbar L_z/(2l_{so}^2)$, thus the total number of states N scales as $L_x L_y L_z^2$. As a result, the 3D local density of states linearly diverges as $\rho_{3D}(z) \propto |z|/l_{so}^4$ as $|z| \to \infty$. Similar divergence also occurs in the symmetric-like gauge as $\rho_{3D}(r) \propto r/l_{so}^4$. Now this seeming pathological result can be understood as the consequence of squeezing states of 4D phase space $(xy; k_x k_y)$ into the 3D real space (xyz). In other words, the correct thermodynamic limit should be taken according to the volume of 4D phase space. This reasoning is easily extended to the 4D LL systems (Eq. (4.88)), which can be understood as a 6D phase space of $(xyz; k_x k_y k_z)$.

4.7.5 *Charge pumping and the 4D quantum Hall effects*

The above 4D Landau-level states presented in Sec. 4.7.3 exhibit nonlinear electromagnetic response [13, 24, 61, 62] as the 4D quantum Hall effect. We apply the electromagnetic fields as

$$\vec{E} = E\hat{z}, \quad \vec{B} = B\hat{z}, \tag{4.92}$$

to the 4D Landau-level Hamiltonian equation (4.88) by minimally coupling fermions to the $U(1)$ vector potential,

$$A_{em,x} = 0, \quad A_{em,y} = Bx, \quad A_{em,z} = -cEt. \tag{4.93}$$

The $\vec{B}$-field further quantizes the chiral plane-wave modes inside the nth 4D spin–orbit Landau-level states into a series of 2D magnetic Landau-level states in the xy-plane as labeled by the magnetic Landau-level index m.

For the case of $m = 0$, the eigen-wavefunctions are spin polarized as

$$\Psi_{n,m=0}(k_y, k_z) = e^{ik_y y + ik_z z}\phi_n(u - u_0(k_z, m = 0))\varphi_{m=0}(x - x_0(k_y)) \otimes | \uparrow\rangle, \tag{4.94}$$

where ϕ_n is the nth order harmonic oscillator wavefunction with the spin–orbit length scale l_{so}, and φ_0 is the zeroth-order harmonic oscillator wavefunction with the magnetic length scale l_B. The central positions of the u-directional and x-directional oscillators are

$$x_0(k_y) = l_B^2 k_y, \quad u_0(k_z, m = 0) = l_{so}^2 k_z, \tag{4.95}$$

respectively. The key point is that $u_0(k_z, m = 0)$ runs across the entire u-axis. In contrast, wavefunctions $\Psi_{n,m}$ with $m \geq 1$ also exhibit harmonic oscillator wavefunctions along the u-axis. However, their central positions at $m \geq 1$ are,

$$u_0(k_z) = \pm l_{so}^2 \sqrt{k_z^2 + \frac{2m}{l_B^2}}, \tag{4.96}$$

which only lie in half of the u-axis as shown in Fig. 4.4(c).

Since k_z increases with time in the presence of E_z, $u_0(m, k_z(t))$ moves along the u-axis. Only the $m = 0$ branch of the magnetic Landau-level states contribute to the charge pumping since their centers go across the entire u-axis, which results in an electric current along the u-direction. Since $k_z(t) = k_z(0) - \frac{eE}{\hbar}t$, during the time interval Δt, the number of electrons passing the cross-section at a fixed u is

$$\Delta N = \frac{L_x L_y}{2\pi l_B^2} \frac{eE_z \Delta t}{2\pi\hbar/L_z} = \frac{e^2}{4\pi^2\hbar^2 c}\vec{E} \cdot \vec{B} V \Delta t, \tag{4.97}$$

where V is the 3D cross-volume. Then the current density is calculated as

$$j_u = n_{occ}\frac{e\Delta N}{V\Delta t} = n_{occ}\alpha\frac{e}{4\pi^2\hbar}\vec{E} \cdot \vec{B}, \tag{4.98}$$

where α is the fine-structure constant, and n_{occ} is the occupation number of the 4D spin–orbit Landau levels.

Equation (4.98) is in agreement with results from the effective field theory [13] as the 4D generalization of the quantum Hall effect. If we impose the open boundary condition perpendicular to the u-direction, the above charge pump process corresponds to the chiral anomalies of Weyl fermions with opposite chiralities on two opposite 3D boundaries, respectively. Since they are spatially separated, the chiral current corresponds to the electric current along the u-direction.

4.8 Conclusions and outlooks

I have reviewed a general framework for constructing Landau levels in high dimensions based on harmonic oscillator wavefunctions. By imposing spin–orbit coupling, their spectra are reorganized to exhibit flat dispersions and nontrivial topological properties. In particular, the lowest Landau-level wavefunctions in 3D and 4D in the quaternion representation satisfy the Cauchy–Riemann–Fueter condition, which is the generalization of complex analyticity to high dimensions. The boundary excitations are the 2D helical Dirac surface modes, or, the 3D chiral Weyl modes. There is a beautiful bulk–boundary correspondence that the Cauchy–Riemann–Fueter condition and the helical Dirac (chiral Weyl) equation are the Euclidean and Minkowski representations of the same analyticity condition, respectively. By dimensional reductions, we constructed a class of Landau levels in 2D and 3D which are time-reversal invariant but parity breaking. The Landau-level problem for Dirac fermions is a square-root problem of the nonrelativistic one, corresponding to complex quaternions. The zeroth-Landau-level states are a flat band of half-fermion Jackiw–Rebbi zero modes. It is at the interface between condensed matter and high-energy physics, related to a new type of anomaly. Unlike parity anomaly and chiral anomaly studied in field theory in which Dirac fermions are coupled to gauge fields through the minimal coupling, here Dirac fermions are coupled to background fields in a nonminimal way.

I speculate that high-dimensional Landau levels could provide a platform for exploring interacting topological states in high dimensions — due to the band flatness, and also the quaternionic analyticity of lowest Landau-level wavefunctions. It would stimulate the developments of various theoretical and numerical methods. This would be an important direction in both condensed matter physics and mathematical physics for studying high-dimensional topological states with both nonrelativistic and relativistic fermions. This research also provides interesting applications of quaternion analysis to theoretical physics.

Appendix A: Brief review on Clifford algebra

In this appendix, we review how to construct anti-commutative Γ-matrices. The familiar group is just the 2×2 Pauli matrices, i.e., rank-1. The rank-k

Γ-matrices can be defined recursively based on the rank-$(k-1)$ ones. At each level, there are $2k+1$ anti-commutative matrices, and their dimensions are $2^k \times 2^k$. In this chapter, we use the following representation:

$$\Gamma_i^{(k)} = \begin{bmatrix} 0 & \Gamma_a^{(k-1)} \\ \Gamma_a^{(k-1)} & 0 \end{bmatrix}, \quad \Gamma_{2k}^{(k)} = \begin{bmatrix} 0 & -iI \\ iI & 0 \end{bmatrix}, \quad \Gamma_{2k+1}^{(k)} = \begin{bmatrix} I & 0 \\ 0 & -I \end{bmatrix}, \tag{A1}$$

where $i = 1, \ldots, 2k-1$.

In $D = 2k+1$-dimensional space, the SO$(2k+1)$ fundamental spinor is 2^k-dimensional. The generators are constructed $S_{ij} = \frac{1}{2}\Gamma_{ij}^{(k)}$ where

$$\Gamma_{ij}^{(k)} = -\frac{i}{2}[\Gamma_i^{(k)}, \Gamma_j^{(k)}]. \tag{A2}$$

In the $D = 2k$-dimensional space, there are two irreducible fundamental spinor representations for the SO$(2k)$ group, both of which are with 2^{k-1}-dimensional. Their generators are denoted as S_{ij} and S'_{ij}, respectively, which can be constructed based on both rank-$(k-1)$ $\Gamma_i^{(k-1)}$ and $\Gamma_{ij}^{(k-1)}$-matrices. For the first $2k-1$ dimensions, the generators share the same form as that of the SO$(2k-1)$ group,

$$S_{ij} = S'_{ij} = \frac{1}{2}\Gamma_{ij}^{(k-1)}, \quad (1 \le i < j \le 2k-1). \tag{A3}$$

Other generators $S_{i,2k}$ and $S'_{i,2k}$ differ by a sign — they are represented by the $\Gamma_i^{(k-1)}$ matrices,

$$S_{i,2k} = S'_{i,2k} = \pm\frac{1}{2}\Gamma_i^{(k-1)}, \quad (1 \le i \le 2k-1). \tag{A4}$$

Acknowledgments

I thank Yi Li for collaborations on this set of works on high-dimensional topological states and for bringing in interesting concepts including the quaternionic analyticity. I also thank J.E. Hirsch for stimulating discussions, and S. C. Zhang, T. L. Ho, E. H. Fradkin, S. Das Sarma, F. D. M. Haldane, and C. N. Yang for their warm encouragements and appreciations. This work is partly supported by AFOSR FA9550-14-1-0168 and NSFC under the Grants No. 11729402.

References

[1] A. Sudbery, Quaternionic analysis, *Math. Proc. Cambridge Philos. Soc.* **85**(2), 199–224 (1979).

[2] S. L. Adler, *Quaternionic Quantum Mechanics and Quantum Fields*. vol. 88 (Oxford University Press, 1995).

[3] D. Finkelstein, Foundations of quaternion quantum mechanics, *J. Math. Phys.* **3**, 207 (1962).

[4] C. N. Yang, *Selected Papers (1945–1980) with Commentary* (World Scientific, 2005).

[5] B. A. Bernevig and S. C. Zhang, Quantum spin Hall effect, *Phys. Rev. Lett.* **96**(10), 106802 (2006).

[6] C. L. Kane and E. J. Mele, $\mathbb{Z}_2$ Topological order and the quantum spin Hall effect, *Phys. Rev. Lett.* **95**(14), 146802, (2005).

[7] C. L. Kane and E. J. Mele, Quantum spin Hall effect in graphene, *Phys. Rev. Lett.* **95**(22), 226801 (2005).

[8] L. Fu and C. L. Kane, Topological insulators with inversion symmetry, *Phys. Rev. B* **76**(4), 045302 (2007).

[9] L. Fu, C. L. Kane and E. J. Mele, Topological insulators in three dimensions, *Phys. Rev. Lett.* **98**(10), 106803 (2007).

[10] J. E. Moore and L. Balents, Topological invariants of time-reversal-invariant band structures, *Phys. Rev. B* **75**(12), 121306 (2007).

[11] B. A. Bernevig, T. L. Hughes, and S. C. Zhang, Quantum spin Hall effect and topological phase transition in HgTe quantum wells, *Science* **314**(5806), 1757 (2006).

[12] C. Wu, B. Bernevig, and S.-C. Zhang, Helical liquid and the edge of quantum spin Hall systems, *Phys. Rev. Lett.* **96**(10), 106401, (2006).

[13] X. L. Qi, T. L. Hughes, and S. C. Zhang, Topological field theory of time-reversal invariant insulators, *Phys. Rev. B* **78**(19), 195424 (2008).

[14] R. Roy, Topological phases and the quantum spin Hall effect in three dimensions, *Phys. Rev. B* **79**(19), 195322 (2009).

[15] R. Roy, Characterization of three-dimensional topological insulators by two-dimensional invariants, *New J. Phys.* **12**, 065009 (2010).

[16] D. J. Thouless, M. Kohmoto, M. P. Nightingale, and M. den Nijs, Quantized Hall conductance in a two-dimensional periodic potential, *Phys. Rev. Lett.* **49**(6), 405 (1982).

[17] F. D. M. Haldane, Model for a Quantum Hall effect without Landau levels: Condensed-matter realization of the "parity anomaly", *Phys. Rev. Lett.* **61**(18), 2015–2018 (1988).

[18] A. Kitaev, Periodic table for topological insulators and superconductors, *Amer. Inst. Phys. Conf. Ser.* **1134**, 22–30 (2009).

[19] A. Schnyder, S. Ryu, A. Furusaki, and A. Ludwig, Classification of topological insulators and superconductors in three spatial dimensions, *Phys. Rev. B* **78**(9), 195125 (2008).

[20] K. Klitzing, G. Dorda, and M. Pepper, New method for high-accuracy determination of the fine-structure constant based on quantized Hall resistance, *Phys. Rev. Lett.* **45**(6), 494–497 (1980).

[21] D. C. Tsui, H. L. Stormer, and A. C. Gossard, Two-dimensional magnetotransport in the extreme quantum limit, *Phys. Rev. Lett.* **48**, 1559 (1982); doi: 10.1103/PhysRevLett.48.1559; URL http://link.aps.org/doi/10.1103/PhysRevLett.48.1559.

[22] S. Girvin, The quantum hall effect: Novel excitations and broken symmetries, *Aspects topologiques de la physique en basse dimension. Topological aspects of low dimensional systems*. pp. 53–175 (1999).

[23] R. Laughlin, Anomalous quantum Hall effect: An incompressible quantum fluid with fractionally charged excitations, *Phys. Rev. Lett.* **50**(18), 1395–1398 (1983).

[24] S. C. Zhang and J. P. Hu, A four-dimensional generalization of the quantum Hall effect, *Science* **294**(5543), 823 (2001).

[25] F. D. M. Haldane, Fractional quantization of the hall effect: A hierarchy of incompressible quantum fluid states, *Phys. Rev. Lett.* **51**(7), 605–608 (1983).

[26] Y. Li, X. Zhou, and C. Wu, Two- and three-dimensional topological insulators with isotropic and parity-breaking Landau levels, *Phys. Rev. B* **85**, 125122 (2012).

[27] Y. Li and C. Wu, High-dimensional topological insulators with quaternionic analytic landau levels, *Phys. Rev. Lett.* **110**, 216802 (2013); doi: 10.1103/PhysRevLett.110.216802; URL https://link.aps.org/doi/10.1103/PhysRevLett.110.216802.

[28] Y. Li, K. Intriligator, Y. Yu and C. Wu, Isotropic Landau levels of Dirac fermions in high dimensions, *Phys. Rev. B* **85**, 085132 (2012).

[29] R. Jackiw and C. Rebbi, Solitons with fermion number $\frac{1}{2}$, *Phys. Rev. D.* **13**, 3398–3409 (1976); doi: 10.1103/PhysRevD.13.3398; URL http://link.aps.org/doi/10.1103/PhysRevD.13.3398.

[30] Y. Li, S.-C. Zhang and C. Wu, Topological insulators with su(2) landau levels, *Phys. Rev. Lett.* **111**, 186803 (2013); doi: 10.1103/PhysRevLett.111.186803; URL https://link.aps.org/doi/10.1103/PhysRevLett.111.186803.

[31] I. Frenkel and M. Libine, Quaternionic analysis, representation theory and physics, *Adv. Math.* **218**(6), 1806–1877 (2008); doi: https://doi.org/10.1016/j.aim.2008.03.021; URL http://www.sciencedirect.com/science/article/pii/S0001870808000935.

[32] A. V. Balatsky, Quaternion generalization of the laughlin state and the three dimensional fractional QHE, Preprint (1992); arXiv:cond-mat/9205006.

[33] G. W. Semenoff, Condensed-matter simulation of a three-dimensional anomaly, *Phys. Rev. Lett.* **53**(26), 2449–2452 (1984).

[34] A. J. Heeger, S. Kivelson, J. R. Schrieffer and W. P. Su, Solitons in conducting polymers, *Rev. Mod. Phys.* **60**, 781–850 (1988); doi: 10.1103/RevModPhys.60.781; URL http://link.aps.org/doi/10.1103/RevModPhys.60.781.

[35] A. N. Redlich, Gauge noninvariance and parity nonconservation of three-dimensional fermions, *Phys. Rev. Lett.* **52**, 18–21 (1984); doi: 10.1103/PhysRevLett.52.18; URL http://link.aps.org/doi/10.1103/PhysRevLett.52.18.

[36] A. N. Redlich, Parity violation and gauge noninvariance of the effective gauge field action in three dimensions, *Phys. Rev. D* **29**, 2366–2374 (1984); doi: 10.1103/PhysRevD.29.2366; URL http://link.aps.org/doi/10.1103/PhysRevD.29.2366.

[37] A. J. Niemi and G. W. Semenoff, Fermion number fractionization in quantum field theory, *Phys. Rep.* **135**(3), 99–193 (1986).

[38] P. Streda, Quantised hall effect in a two-dimensional periodic potential, *J. Phys. C: Solid State Phys.* **15**(36), L1299 (1982); URL http://stacks.iop.org/0022-3719/15/i=36/a=006.

[39] B. K. Bagchi, *Supersymmetry in Quantum and Classical Mechanics* (Chapman & Hall/CRC, 2001).

[40] D. H. Lee and C. L. Kane, Boson-vortex-skyrmion duality, spin-singlet fractional quantum hall effect, and spin-1/2 anyon superconductivity, *Phys. Rev. Lett.* **64**, 1313–1317 (1990); doi: 10.1103/PhysRevLett.64.1313; URL http://link.aps.org/doi/10.1103/PhysRevLett.64.1313.

[41] S. L. Sondhi, A. Karlhede, S. A. Kivelson and E. H. Rezayi, Skyrmions and the crossover from the integer to fractional quantum hall effect at small zeeman energies, *Phys. Rev. B* **47**(24), 16419 (1993).

[42] H. A. Fertig, L. Brey, R. Côté and A. H. MacDonald, Charged spin-texture excitations and the hartree-fock approximation in the quantum hall effect, *Phys. Rev. B* **50**, 11018–11021 (1994); doi: 10.1103/PhysRevB.50.11018; URL http://link.aps.org/doi/10.1103/PhysRevB.50.11018.

[43] N. Read and S. Sachdev, Continuum quantum ferromagnets at finite temperature and the quantum hall effect, *Phys. Rev. Lett.* **75**, 3509–3512 (1995); doi: 10.1103/PhysRevLett.75.3509; URL http://link.aps.org/doi/10.1103/PhysRevLett.75.3509.

[44] F. D. M. Haldane and E. H. Rezayi, Finite-size studies of the incompressible state of the fractionally quantized hall effect and its excitations, *Phys. Rev. Lett.* **54**, 237–240 (1985); doi: 10.1103/PhysRevLett.54.237; URL http://link.aps.org/doi/10.1103/PhysRevLett.54.237.

[45] R. E. Prange and S. M. Girvin, Eds., *The Quantum Hall Effect*, 2nd edn. (Springer-Verlag, New York, 1990).

[46] D. Haldane, Geometrical description of the fractional quantum Hall effect, *Phys. Rev. Lett.* **107**, 116801 (2011).

[47] T. Can, M. Laskin, and P. Wiegmann, Fractional quantum Hall effect in a curved space: Gravitational anomaly and electromagnetic response, *Phys. Rev. Lett.* **113**(4), 046803 (2014); doi: 10.1103/PhysRevLett.113.046803.

[48] S. Klevtsov, X. Ma, G. Marinescu and P. Wiegmann, Quantum Hall effect and quillen metric, *Commun. Math. Phys.* **349**(3), 819–855 (2017); doi: 10.1007/s00220-016-2789-2.

[49] C. J. Wu, I. Mondragon-Shem and Z. Xiang-Fa, Unconventional Bose–Einstein condensations from spin–orbit coupling, *Chinese Phys. Lett.* **28**(9), 097102 (2011); URL http://stacks.iop.org/0256-307X/28/i=9/a=097102.

[50] Y. Li, X. Zhou and C. Wu, Three-dimensional quaternionic condensations, hopf invariants, and skyrmion lattices with synthetic spin–orbit coupling, *Phys. Rev. A* **93**, 033628 (2016); doi: 10.1103/PhysRevA.93.033628; URL https://link.aps.org/doi/10.1103/PhysRevA.93.033628.

[51] C. Wu and I. Mondragon-Shem, Exciton condensation with spontaneous time-reversal symmetry breaking, Preprint (2008); arXiv:0809.3532v1.

[52] X. Zhou, Y. Li, Z. Cai and C. Wu, Unconventional states of bosons with the synthetic spin–orbit coupling, *J. Phys. B Atomic Molecular Phys.* **46**(13), 134001 (2013); doi: 10.1088/0953-4075/46/13/134001.

[53] H. Hu, B. Ramachandhran, H. Pu and X. J. Liu, Spin–orbit coupled weakly interacting bose-einstein condensates in harmonic traps, *Phys. Rev. Lett.* **108**, 010402 (2012); doi: 10.1103/PhysRevLett.108.010402; URL http://link.aps.org/doi/10.1103/PhysRevLett.108.010402.

[54] S. Sinha, R. Nath and L. Santos, Trapped two-dimensional condensates with synthetic spin–orbit coupling, *Phys. Rev. Lett.* **107**, 270401 (2011); doi: 10.1103/PhysRevLett.107.270401; URL http://link.aps.org/doi/10.1103/PhysRevLett.107.270401.

[55] S. K. Ghosh, J. P. Vyasanakere and V. B. Shenoy, Trapped fermions in a synthetic non-abelian gauge field, *Phys. Rev. A* **84**, 053629 (2011); doi: 10.1103/PhysRevA.84.053629; URL http://link.aps.org/doi/10.1103/PhysRevA.84.053629.

[56] Z. Wang, X.-L. Qi and S.-C. Zhang, Equivalent topological invariants of topological insulators, *New J. Phys.* **12**, 065007 (2010).

[57] T.-L. Ho and S. Zhang, Bose–Einstein condensates with spin–orbit interaction, *Phys. Rev. Lett.* **107**, 150403 (2011); doi: 10.1103/PhysRevLett.107.150403; URL http://link.aps.org/doi/10.1103/PhysRevLett.107.150403.

[58] D. Xiao, M. Chang and Q. Niu, Berry phase effects on electronic properties, *Rev. Mod. Phys.* **82**, 1959–2007 (2010).

[59] C. G. Callan and J. A. Harvey, Anomalies and fermion zero modes on strings and domain walls, *Nuc. Phys. B* **250**, 427–436 (1985); doi: 10.1016/0550-3213(85)90489-4; URL http://www.sciencedirect.com/science/article/pii/0550321385904894.

[60] D. H. Lee and J. M. Leinaas, Mott insulators without symmetry breaking, *Phys. Rev. Lett.* **92**, 096401 (2004); doi: 10.1103/PhysRevLett.92.096401; URL http://link.aps.org/doi/10.1103/PhysRevLett.92.096401.

[61] P. Werner, (4+1)-dimensional quantum hall effect & applications to cosmology, Preprint (2012); arXiv:1207.4954.

[62] J. Fröhlich and B. Pedrini, New applications of the chiral anomaly, Preprint (2000); arXiv:hep-th/0002195.